Autocrine insulin pathway signaling regulates actin dynamics in cell wound repair

Mitsutoshi Nakamura[1,*], Andrew N.M. Dominguez[1,*], Jeffrey M. Verboon[1,*], Maria Teresa Abreu-Blanco[1], Raymond Liu[1], Jeffrey J. Delrow[2] and Susan M. Parkhurst[1,†]

[1]Basic Sciences Division and [2]Genomics Shared Resource, Fred Hutchinson Cancer Research Center, Seattle, WA, USA 98109

Running Title:

Key Words: cell wound healing, cytoskeleton, insulin signaling, transcription, translation, Drosophila

*Authors contributed equally.

[†]Corresponding author: Fred Hutchinson Cancer Research Center, 1100 Fairview Ave N., A1-187, Seattle, WA, 98109, USA. Phone: (206) 667-6466; E-mail: susanp@fredhutch.org

Abstract

Cells are exposed to frequent mechanical and/or chemical stressors that can compromise the integrity of the plasma membrane and underlying cortical cytoskeleton. The molecular mechanisms driving the immediate repair response that is launched to restore the cell cortex and circumvent cell death are largely unknown. Using drug-inhibition studies and microarray analyses in the *Drosophila* model, we find that initiation of cell wound repair is dependent on translation, whereas transcription is required for subsequent steps in the process. We identified 253 genes whose expression is up-regulated (80) or down-regulated (173) in response to laser wounding. A subset of these genes were validated using RNAi knockdowns and found to exhibit aberrant actomyosin ring assembly and/or actin remodeling defects. Strikingly, we find that disruption of the canonical insulin signaling pathway leads to abnormal wound repair, and that it controls actin dynamics through the actin regulators Girdin and Chickadee (profilin). Our results provide new insight for understanding how cell wound repair proceeds in healthy individuals and those with diseases involving wound healing deficiencies.

Introduction

Numerous cell types in the body are subject to high levels of stress daily. These stresses—physiological and/or environmental—can cause ruptures in the plasma membrane and its underlying cytoskeleton, requiring a rapid repair program to avert further damage, prevent infection/death, and restore normal function (Andrews and Corrotte, 2018; Bement et al., 2007; Draeger et al., 2014; Gurtner et al., 2008; McNeil and Kirchhausen, 2005; McNeil and Terasaki, 2001; Moe et al., 2015; Nakamura et al., 2018; Sonnemann and Bement, 2011; Tang and Marshall, 2017; Velnar et al., 2009). Injuries to individual cells can also occur as a result of accidents/trauma, clinical interventions, and disease conditions, including diabetes, skin blistering disorders, and muscular dystrophies, as well as in response to pore forming toxins secreted by pathogenic bacteria (Clarke et al., 1995; Cooper and McNeil, 2015; Coulombe et al., 1991; Galan and Bliska, 1996; Petrof et al., 1993). Repair of these cell cortex lesions can be particularly troublesome when occurring alongside these fragile cell disease states or in a non-renewing and/or irreplaceable cell type. Thus, the importance of cell cortex continuity and delineating the molecular mechanisms regulating cell wound repair is of considerable clinical relevance, and important for advancing our knowledge of the many critical cell behaviors and fundamental regulations underpinning normal biological events that are co-opted for this repair process.

Aspects of single cell wound repair dynamics have been studied in *Xenopus* oocytes, sea urchin eggs, mammalian tissue culture cells, and the genetically-amenable *Drosophila* syncytial embryo (Abreu-Blanco et al., 2011a, b; Bement et al., 1999; Kono et al., 2012; Nakamura et al., 2018; Steinhardt et al., 1994; Terasaki et al., 1997; Yumura et al., 2014). This repair is generally conserved among these organisms and occurs in four main phases (Figure 1A). In the first phase, the wound expands as the cell recognizes the membrane breach and subsequently forms a membranous plug to neutralize any flux between the extracellular space and cytoplasm. Second, the cell constructs an actomyosin ring that underlies the plasma membrane at the wound edge. Third, the actomyosin ring translocates inward to draw the wound area closed. Mechanistic variations exist during this step wherein the actomyosin ring in some models translocates through actin treadmilling (actin simultaneously polymerizes at the inner edge and depolymerizes at the outer edge of the actin ring), while others use myosin II for sarcomere-like contraction (anti-parallel actin filaments are directed past each other in opposing directions) (Abreu-Blanco et al., 2011a, b, 2014; Benink and Bement, 2005; Burkel et al., 2012; Nakamura et al., 2018). The final step of wound repair occurs in which the plasma membrane and the underlying cortical

cytoskeleton are remodeled returning them to their pre-wounded composition and organization. The mechanisms deployed by the cell for this remodeling have not yet been delineated.

Previous studies have shown that Ca^{2+} is required for the initiation of cell wound repair and serves as a messenger to trigger downstream processes such as transcription: release of internal and/or external Ca^{2+} stores activates a number of intracellular pathways resulting in an uptick of gene expression (Fein and Terasaki, 2005; Grembowicz et al., 1999; Joost et al., 2018; Togo, 2004). Studies carried out in rat embryos and cultured bovine aortic endothelial cells showed a rapid increase in expression of the Ca^{2+}-responsive element containing c-Fos protein as a direct result of plasma membrane damage (Grembowicz et al., 1999; Martin and Nobes, 1992; Verrier et al., 1986). c-Fos, a component of the Activator protein 1 (AP-1), serves as a transcription factor responsible for expressing a number of cytokines and growth factors required to drive the appropriate cellular responses necessary for wound recovery (Shaulian and Karin, 2002; Yates and Rayner, 2002).

Interestingly, though the *Drosophila* syncytial embryo functions under the developmental control of maternally-contributed mRNAs and proteins with minimal levels of zygotic transcription, it is still able to immediately recognize and repair breaches to its cortex. Here we show that translation, rather than transcription, is required for the initial stages of repair in this cell wound repair model. Although transcription does not serve as a “start” signal, disrupting transcription leads to impaired repair in subsequent steps of the process. Using microarrays to assess gene expression changes post-wounding, we have identified 253 genes with a potential role in cell wound repair, indicated by changes in their expression—either up or down—in response to laser wounding. A subset of these genes were analyzed using RNAi knockdowns to visualize spatio-temporal patterns that verified their involvement. Strikingly, we find that the canonical insulin signaling pathway is required for proper cell wound repair where it controls actin dynamics through the actin regulators Girdin (Hook-like protein family) and Chickadee (profilin). Thus, our study provides insight into the roles of transcription, translation, and insulin signaing in cell wound repair and provides new avenues for understanding how wound healing proceeds in healthy individuals and disease sufferers with wound healing impairments.

Results

Assessment of transcriptional contribution to cell wound repair. To investigate the role of transcription in cell wound repair using the *Drosophila* syncytial (nuclear cycle 4-6) embryo model, we performed a microarray screen on full-length cDNA arrays to compare changes of gene expression between laser wounded and non-wounded states at two time points: immediately after wounding (0-5 minutes post-wounding (mpw)) and at the end of the repair process (~30 mpw) (Figure 1B). We found that at the immediate timepoint, wounded embryos exhibited no significant changes in their expression profiles when compared to their non-wounded counterparts (Figure 1C). Interestingly, the later timepoint showed significant changes of gene expression in both the up and down directions (Figure 1D). Using a false discovery rate of 0.05, we identified 253 genes with statistically significant changes: 80 that are up-regulated and 173 that are down-regulated (Table 1; Table S1). The robustness of the differences we observe is striking given that only ~5-10% of the cell surface is wounded and undergoing repair.

We next determined if these genes were being co-differentially expressed by shared activating or regulatory elements within a localized region of the genome in response to wounding. Genome mapping of the 253 genes show no obvious clustering upon visual inspection (Figure 1E). Concomitantly, we mapped the 253 differentially-expressed genes onto the 1169 unique topologically associated domains (TADs) previously characterized in flies(Li et al., 2017), and found no difference in overall differentially-expressed genes between TADs (p=0.22), as well as when comparing just the down-regulated genes (p=0.81) (Figure 1F). Interestingly, we detected a slight difference in differentially-expressed genes by TAD for up-regulated genes (p=0.01), however the majority of this signal appears to be driven by TADs that were missing genes due to their poorer coverage on our arrays. The results from this TAD analysis suggest that the 253 genes are being regulated independently and deliberately in response to wound repair. Intriguingly, the 80 upregulated genes were, on-average, larger than gene products previously recorded during this stage of development (Figure 1G) (Artieri and Fraser, 2014; Fukaya et al., 2017; Sandler et al., 2018; Vastenhouw et al., 2019), implicating the existence of a wound-repair specific program (see Discussion).

Transcription is not required to initiate cell wound repair. We expected that if transcription served as an initiator for wound repair as previously proposed, then inhibition of transcriptional activity would result in disrupted actin dynamics throughout the wound repair process. From our initial microarray results, we observe significant changes in gene expression exclusively at the

later timepoint indicating that transcriptional activity is not necessary for initiating the wound repair process in this model. To further delineate the role of transcription in this process, we wounded nuclear cycle 4-6 *Drosophila* embryos that were injected with α-amanitin, a transcription inhibitor that targets RNA polymerase thereby halting transcritional activity, and that also expressed an actin-GFP reporter (sGMCA) to observe wound repair dynamics using time-lapse microscopy. In control embryos, where only buffer was injected, actin became enriched in two distinct locations: 1) adjacent to the wound edge, forming a robust actin ring, and 2) in a "halo" or diffuse accumulation along the outer periphery of the ring (Figure 2A-A',D-F; Video 1). Consistent with our microarray results, α-amanitin injected embryos initially showed actin dynamics similar to those observed in control embryos, however they exhibited disruptions to the repair process during the subsequent actin remodeling phases (Figure 2B-B', D-F; Video 1). To ensure that we were getting efficient transcriptional knockdown, we verified the efficacy and duration of the α-amanitin treatment using the MS2-MCP system, a visual reporter of active transcription (see Methods) (Figure 2G-I') (Forrest and Gavis, 2003; Weil et al., 2006). In *Drosophila* syncytial embryos, GFP appears as puncta within the nuclei of control embryos indicative of active transcription, whereas these GFP puncta are absent in α-amanitin injected embryos indicating that α-amanitin is effective in inhibiting transcription even beyond our initial wounding window (Figure 2H-H'; Video1). Thus, our results indicate that a transcriptional response is dispensable for the initiation of cell wound repair in the *Drosophila* model, but becomes important subsequently, potentially for replenishing and/or maintaining various factors necessary for establishing the wound repair response.

The initial steps of cell wound repair are translation dependent. *Drosophila* early embryonic development is mostly driven by maternally deposited mRNA and protein until the maternal-to-zygotic genome transition (MZT) at nuclear cyle 14 (cf. (Vastenhouw et al., 2019)). To explore what role translation might be playing in driving the wound repair process, embryos expressing a fluorescent actin reporter (sGMCA) were injected with the translation inhibitor puromycin prior to laser wound induction. After the initial formation of an actin ring (~2 mins), the ring began to disassemble while actin simultaneously became enriched inside the wound area (Figure 2C-C'). Quantitative measurements show a prolonged wound healing process compared to controls (Figure 2D), with significantly less wound expansion and slower wound closure (Figure 2E-F). Taken together, our results suggest that the *Drosophila* embryo requires active translation to initiate wound repair, as well as to regulate actin dynamics throughout the repair process.

Knockdown of differentially expressed genes results in wound over-expansion and abnormal actin dynamics upon wounding. We next examined the effects of removing the differentially-expressed genes on cell wound repair. We generated knockdown embryos for 15 of the top 16 up-regulated genes and the 16 top down-regulated genes (based on their fold-change; Table 1) by expressing RNAi constructs in the female germline using the GAL4-UAS system (Brand and Perrimon, 1993; Rorth, 1998), then observing actin dynamics using a fluorescent actin reporter (sGMCA).

UP-REGULATED GENES. In all 15 cases of RNAi knockdown for up-regulated genes, wounded embryos exhibited abnormal actin dynamics that fell within three major visually distinct, but non-mutually exclusive, classes: 1) premature actin ring/halo disassembly, 2) failure of actin ring/halo dissassembly, and 3) abnormal actin ring/halo disassembly with concomitant accumulation of actin within the wound (Figure 3; Video 2; Figure S1). Among CLASS 1 members, exemplified by their incomplete formation and premature dissassembly of the actomyosin ring causing rifts at the initial injury site that remained open for the entire time of repair, are Imaginal morphogenesis protein-Late 2 (ImpL2) and Epidermial growth factor receptor (EGFR) (Figure 3B-C',J-K; Video 2). ImpL2 has been proposed to work antagonisitically to the insulin/insulin-like (IIS) signaling pathway by interacting with receptor/ligand interactions to inhibit downstream signal transduction (Amoyel et al., 2016; Figueroa-Clarevega and Bilder, 2015; Kwon et al., 2015). EGFR encodes a receptor tyrosine kinase that works upstream of the c-jun N-terminal kinase (JNK) and decapentaplegic (dpp) pathways. Loss of EGFR results in down-regulation of JNK activity leading to the impairment of dorsal closure, a process sharing many features with epithelial (multicellular) wound repair (Kushnir et al., 2017).

CLASS 2 members, exemplified by Gp150, Inx3, and Thor, are unable to resolve actin structures or properly remodel cortical actin after wound closure (Figure 3D-F',L-N; Video 2). Gp150 encodes a transmembrane glycoprotein that regulates Notch signaling during normal eye development in *Drosophila (Li et al., 2003)*, whereas Inx3 encodes a gap junction protein involved in morphogenesis and nervous system development (Giuliani et al., 2013; Lautemann and Bohrmann, 2016). Thor encodes a translation inhibitor functioning downstream of insulin signaling that is sensitive to reactive oxygen species (Toshniwal et al., 2019). Interestingly, like ImpL2, Thor is a IIS pathway constituent and Gp150 has also been shown to physically interact with components of this pathway (Pten and S6k) (Vinayagam et al., 2016).

CLASS 3 genes, exemplified by Jitterbug (Jbug) and Nullo, are characteristically defined by the pronounced formation of actin inside the wound area (Figure 3G-H',O-P; Video 3). Jbug is a filamin-type protein that serves as an F-actin crosslinker providing stability to the cytoskeleton, a

system that has been proposed to utilize mechanical cues such as tension to modulate cellular processes (Martino et al., 2018; Nakamura et al., 2011). Nullo has been shown to establish cortical compartments during cellularization of the *Drosophila* embryo, suggesting an important role regulating actin stability at the cortex (Sokac and Wieschaus, 2008a, b).

DOWN-REGULATED GENES. Interestingly, in all 16 cases of RNAi knockdown for the down-regulated genes examined, wounded embryos exhibited abnormal actin dynamics that fell within the same three major distinct, but non-mutually exclusive, categories as described above for the up-regulated genes. A number of the genes that were downregulated have an unknown molecular function and/or associated biological processes (Table 1; Figure 4; Video 3; Figures S1q, S2). Of these unknown genes, CG31075, CG4960, and CG1598 exhibited characteristics of CLASS 1, CLASS 2, and CLASS 3 phenotypes, respectively. CG31075 underwent a mild expansion followed by a severly slowed closure rate and incomplete wound closure (Figure 4A-A',H; Video 3), CG4960 exhibited a slight delay in wound repair dynamics but retained noticably enriched actin structures after closure (Figure 4E-E',L; Video 3), and CG1598 developed a visually distinct, but transient, enrichment of actin inside the wound area prior to closure (Figure 4G-G',N; Video 3). Of genes with known motifs/functions, Glutatione S transferases D2 (GstD2) and D1 (GstD1) mutants showed nearly identical phenotypes exhibiting a short-lived accumulation of actin inside the wound area and prolonged closure dynamics during the initial steps of repair (Figure 4B-B',F-F',I,M; Video 3), but in later steps GstD1 was unable to completely close (Figure 4B-B',I; Video 3). Wound repair begins normally in *exu* knockdowns, however the leading edge and surrounding actin structures soon become static resulting in an open wound area and prolonged actin accumulation (Figure 4D-D',K; Video 3). In addition to the phenotypes described above, many of these knockdowns exhibit wound over-expansion (Impl2, EGFR, Gp150, Thor, Dpn, l(3)neo38, GstD1, GstD2, CG1598, CG3652, Pex11, Cyp6a9, ReepB, P32, and RpL23) (Figures 3, 4; Videos 3, 4; Figures S1, S2). Thus, in all 31 cases of up- or down- regulated genes examined, knockdown using RNAi transgenes resulted in abnormal cell wound repair. Despite the molecular functions of many of these genes being unknown, they have been implicated in various cellular processes, but most notably insulin signaling.

Activation of insulin/insulin-like (IIS) constituents during normal wound repair. The fact that ImpL2 and Thor, two of the most upregulated genes in our analyses, are constituents of the insulin/insulin-like growth factor signaling (IIS) pathway in *Drosophila* (Figure 5A) was unexpected. Deficiencies in insulin signaling have been implicated in multicellular (tissue) repair, where it is thought to impede growth factor production, angiogenic response, and epidermal

barrier function (Brem and Tomic-Canic, 2007; Galiano et al., 2004; Kakanj et al., 2016; Manzano-Nunez et al., 2019), functions that might not normally be expected to govern regulation within individual cells.

To determine if the canonical IIS pathway was involved in individual cell wound repair, we first examined the recruitment pattern of a PIP_3 (phosphatidylinositol (3,4,5)-triphosphate) GFP-reporter construct used as a reporter of insulin signaling activity (Britton et al., 2002) co-expressed with a Cherry fluorescently-tagged actin reporter (sChMCA) in a wildtype and *chico* RNAi knockdown background (Figure 5B-E). PIP_3 is a phospholipid that composes a subset of specialized plasma membrane with various trafficking and signaling related functions (Rameh and Cantley, 1999). PIP_3 is recruited to same region as the actomyosin ring in wildtype embryos (Figure 5B-B",D), confirming the requirement for autocrine insulin pathway signaling. Importantly, this recruitment is dependent on the upstream activation of the insulin receptor (InR), as PIP_3 recruitment is disrupted in a *chico* RNAi background (Figure 5C-C",E).

We next examined the wound repair phenotypes in knockdown backgrounds for components spanning the IIS pathway by expressing RNAi constructs for pathway components in the female germline using the GAL4-UAS system (Brand and Perrimon, 1993; Rorth, 1998), then observing actin dynamics using a fluorescent actin reporter (sGMCA). The one ligand and six of the major IIS pathway components tested — Ilp4 (Insulin-like peptide), InR (Insulin receptor), Chico (IRS homolog), Pi3K21B (Phosphoinositide3-Kinase), Akt1 (Kinase), FoxO (transcription factor), and Reptor (transcription factor) — exhibited abherrant wound repair with notably similar phenotypes (Figures 5A, 6; Video 4; Figure S1Q). With the exception of InR, mutants for IIS pathway components exhibited wound overexpansion immediately after laser ablation that was visible as the outward retraction of the wound edge (Figure 6, yellow arrows; Video 4). Following this overexpansion, actin structures became transiently enriched inside the wound area, but dissassembled prior to complete wound closure (Figure 6, yellow arrowheads; Video 4). Lastly, progression of wound closure was signficantly delayed and/or incomplete, leaving openings around the actin ring as it translocated (Figure 6, red arrowheads; Video 4). Collectively, these results show that key components of insulin signaling are not only called to a wound, but have detrimental effects on actin dynamics upon knockdown, suggesting that there exists a tight association between the factors that regulate both insulin signaling and cell wound repair in the *Drosophila* model.

The IIS pathway effectors Profilin (Chickadee) and Girdin are required for cell wound repair. The IIS pathway has recently been shown to control actin dynamics independently of its

role in growth control (Ghiglione et al., 2018). In particular, the IIS pathway has been found to activate the expression of the *Drosophila* profilin homolog, Chickadee, as well as the Akt substrate Girdin (GIRDers of actIN; also known as GIV) (Ghiglione et al., 2018; Hartung et al., 2013; Lopez-Sanchez et al., 2015). To determine if these actin regulators function as IIS pathway effectors during cell wound repair, we stained wounded embryos that expressed a GFP-tagged actin reporter (sGMCA) in a wildtype or *chico* RNAi knockdown background with antibodies to Profilin and Girdin (Figure 7A-D). Both proteins are recruited to wounds. Girdin exhibits a punctate recuitment at wounds with the highest accumulation overlapping the membrane plug inside the actin ring and with lower level diffuse accumulation overlapping the actin ring and the innermost part of the actin halo (Figure 7A-B). Profilin recruitment is internal to the actin ring and appears to be excluded from the actin ring region (Figure 7A-B). Importantly, the accumulation of both Girdin and Profilin at wounds requires a functioning IIS pathway as these accumulations are lost in a *chico* RNAi background (Figure 7C-D).

We next examined the effects of removing Girdin and Profilin on cell wound repair. Similar to knockdown of IIS pathway components described above, Girdin RNAi knockdown embryos exhibited aberrant wound repair including wound overexpansion, enrichment of actin structures inside the wound area, and signficantly delayed wound closure (Figure 7E-E',G; Video 4; Figure S1Q). Unfortunately, Profilin RNAi knockdown females do not produce eggs. We therefore used the *wimp* mutation (Parkhurst and Ish-Horowicz, 1991; Verboon et al., 2018) to generate reduced Profilin expression in both the germline and soma (*wimp* reduces maternal gene expression such that, when *in trans* to the *chickadee*^{221} allele, it effectively generates a strong *chickadee* hypomorph, referred to as reduced Profilin). Similar to knockdown of Girdin and IIS pathway components, reduced Profilin embryos exhibited wound overexpansion, enrichment of actin structures inside the wound area, and signficantly delayed wound closure (Figure 7F-F',H; Video 4; Figure S1Q). Thus, our results indicate that Girdin and Profilin are actin regulatory downstream effectors of the IIS pathway in cell wound repair.

Discussion

Our study shows that cellular wound repair is not dependent on transcriptional activity to initiate wound repair programs, that dormant transcription pathways are activated in response to wounds, and that the insulin signaling pathway is an essential component of the repair process. A calcium influx-triggered transcriptional response is thought to be important to lead off the cell wound repair process, eliciting a downstream wound repair program. This proposed mechanism was at odds with the *Drosophila* syncytial embryo cell wound model that faithfully recapitulates the majority of features associated with other single cell wound repair models (*Xenopus* oocytes, tissue culture cells, sea urchin eggs) (Abreu-Blanco et al., 2011a, 2014; Bi et al., 1995; Miyake and McNeil, 1995; Nakamura et al., 2018; Nakamura et al., 2017; Sonnemann and Bement, 2011; Steinhardt et al., 1994; Verboon and Parkhurst, 2015), yet represents a special system running mostly off of maternally contributed products, highlighted by rapid cell cycles (~10 minutes/cycle) and minimal zygotic transcription (Foe and Alberts, 1983; Sandler et al., 2018; Vastenhouw et al., 2019).

Consistent with the closed nature of the *Drosophila* syncytial embryo cell wound model, we find no altered gene expression immediately upon wounding as assayed by microarray analysis of laser wounded versus unwounded embryos or following injection of the α-amanitin transcriptional inhibitor. We do detect alterations in gene expression at subsequent stages in the repair process: we identified 253 genes (out of ~8000 genes assayed) whose expression is significantly up (80 genes) or significantly down (173 genes) following laser wounding.

Polymerase rates in the early *Drosophila* embryo were reported to be 1.1-1.5 kb/min, leading to the suggestion that any genes transcribed in the early *Drosophila* embryo prior to the mid-blastula transition must be small with minimal introns due to the rapid (~10 min) cell cycles and limited transcription time (Ardehali et al., 2009; Garcia et al., 2013; O'Farrell, 1992; Sandler et al., 2018; Shermoen and O'Farrell, 1991; Thummel et al., 1990; Vastenhouw et al., 2019; Yao et al., 2007). Recent studies have revised this rate to 2.4-3.0 kb/min, lowering the size constraints on the zygotic genes that can be successfully transcribed prior to the mid-blastula transition(Fukaya et al., 2017). Therefore, genes up to ~20-25 kb could theoretically be transcribed during the early and rapid *Drosophila* embryo cell cycles. In this case however, the number of mRNA molecules would be likely limited by the overall nuclear cycle due to the lower number of nuclei present and thus copies of DNA.

We find that the average size of transcripts in syncytial *Drosophila* embryos is 2.5 kb, similar to the previously reported size of 2.2 kb (compared to the overall average length of coding genes in *Drosophila* of 6.1 kb) (Artieri and Fraser, 2014; Hoskins et al., 2011). Genes whose expression

goes down during wound repair are, on average, 1.9 kb. It intriguing that these actively down-regulated genes negatively impact the wound repair process when knocked-down. These genes likely represent RNAs stored in the embryo that are used up during the repair process and not replaced. Alternatively, it is possible that wound repair itself may slightly delay development leading to a subset of zygotically expressed genes whose expression is lagging behind in wounded versus unwounded embryos such that this delayed developmental upregulation is read out as a down-regulation of genes.

Surprisingly, we find that genes whose expression is higher after wounding are much larger on average (3.7 kb) than the average sized transcript at that stage (2.5 kb). These genes likely encode cellular components that were expended during the repair process and are being replenished for normal developmental events to proceed, or that are activated specifically for the repair process. This subset of "up-regulated" genes includes genes that are not usually expressed in the early embryo (e.g., CG43693). Thus, our results suggest that, when wounded, the embryo may be able to activate a transcriptional program that is usually dormant during these stages.

Interestingly, 2 of the top 3 genes whose expression is significantly higher following wounding—Impl2 and Thor—are components of the Insulin signaling pathway. While it has been shown that defective insulin signaling impairs epithelial (multicellular) wound repair (Brem and Tomic-Canic, 2007; Galiano et al., 2004; Kakanj et al., 2016; Manzano-Nunez et al., 2019), this result was unexpected for wound repair in single cells. Using a combination of RNAi knockdowns and GFP reporters, we have shown that all major components of the IIS pathway are involved in cellular wound repair and upon knockdown display similar phenotypes, suggesting that in this context the canonical IIS pathway activation occurs in an autocrine-like manner. Previous studies have highlighted the necessity of calcium influx to facilitate vesicle exocytosis and subsequent fusion of the plasma membrane during wound repair (Bi et al., 1995; Miyake and McNeil, 1995; Steinhardt et al., 1994; Terasaki et al., 1997). Similarly, this influx has also been shown to modulate insulin secretion in β-islet cells via the opening of L-type channels by establishing calcium microdomains along the cortex (Lee et al., 2018; Rutter et al., 2006). Insulin/insulin-like peptides are secreted into the extracellular space where they bind to InR thereby activating the heavily conserved IIS pathway that is known to regulate a number of downstream processes that range from transcription via phosphorylation events on the FOXO family of transcription factors to translation via the regulation of the 4E-binding protein, Thor (Brunet et al., 1999; Haeusler et al., 2018; Puig and Tjian, 2005; Teleman et al., 2005). Recently emerging evidence has also shown that the activated IIS pathway can control actin dynamics through activation of actin

371 regulators including Chickadee (profilin) and Girdin (Ghiglione et al., 2018; Hartung et al., 2013;
372 Houssin et al., 2015; Lopez-Sanchez et al., 2015; Wang et al., 2018a).

373 Observation of actin dynamics in mutants for a number of the IIS pathway components show
374 common phenotypes of impaired cytoskeleton dynamics, most notably an immediate over-
375 expansion of the wound leading edge and a transient actin structure forming inside the wound
376 area suggesting that normal wound repair processes are heavily reliant on a functioning IIS
377 pathway. We propose that the initial inrush of calcium generates microdomains that trigger the
378 secretion of the *Drosophila* insulin-like peptide 4 (Ilp4) into the perivitelline space where it
379 recognizes and binds to the extracellular face of the Insulin receptor (Figure 7I, steps 1-4).
380 Subsequently, the InR is activated and initiates a signaling cascade that regulates a number of
381 downstream processes, including cytoskeletal dynamics. Chickadee/profilin binds to actin and
382 affects the formation/remodeling of actin-rich structures (Ghiglione et al., 2018). Girdin also binds
383 to actin, as well as the catenin-cadherin complex and the Exo-70 subunit of the exocyst complex,
384 where it has been proposed to coordinate cytoskeleton organization, cell adhesion, membrane
385 trafficking events, and serves as an indicator for poor prognosis with invasive breast cancers
386 (Choi et al., 2017; Hartung et al., 2013; Houssin et al., 2015; Lopez-Sanchez et al., 2015; Wang
387 et al., 2018b). Interestingly, *girdin* and Profilin knockdown embryos exhibit wound repair
388 phenotypes consistent with defects in actin structure assembly/remodeling, actomyosin ring
389 attachment to the overlying plasma membrane, and membrane trafficking. In addition to the genes
390 involved in the IIS pathway, our microarray analyses identified numerous other genes that show
391 phenotypes associated with actin dynamics regulation. For example, Nullo is a known regulator
392 of actin-myosin stability and has been proposed to affect actin-actin and actin-membrane
393 interactions at the cortex, suggesting a role in cortical remodeling during actomyosin ring
394 contraction (Sokac and Wieschaus, 2008a, b).

395 In summary, our understanding of the mechanisms that trigger cell wound repair remain
396 incomplete, but here we show functional translation is essential for initiating a normal and
397 processive wound repair process, suggesting that the first responders are likely mRNA and
398 protein already present in the cell. While transcription is not immediately necessary in the
399 *Drosophila* cell wound model, it is needed for the repair process. The requirement for insulin
400 signaling in the single cell wound repair context highlights the conservation of repair mechanisms
401 employed. Given its prominence in the single cell, as well as multicellular (tissue), repair
402 pathways, it is not surprising that impaired insulin signaling leads to major wound repair defects
403 in diseases such as diabetes where chronic wounds are symptomatically observed. As many of
404 the top up- and down- regulated genes we identified are evolutionarily conserved genes, but of

405 currently unknown function, the challenge for the future is to determine their roles in normal
406 cellular maintenance and/or development, in addition to their effects in a cell wound repair context,
407 thereby allowing the establishment of a network of cellular processes involved to better aid in
408 treatments of disease involving wound healing impairments, or in disciplines such as regenerative
409 medicine.
410

411 **Materials and Methods**

412

413 **Fly stocks and genetics**

414 Flies were cultured and crossed at 25°C on yeast-cornmeal-molasses-malt extract medium. The
415 flies used in this study are listed in Table S2A. RNAi lines were driven using the GAL4-UAS
416 system using the maternally expressed driver, Pmatalpha-GAL-VP16V37. All genetic fly crosses
417 were performed at least twice. All RNAi experiments were performed at least twice from
418 independent genetic crosses and ≥10 embryos were examined unless otherwise noted.

419 An actin reporter, sGMCA (spaghetti squash driven, moesin-alpha-helical-coiled and actin
420 binding site bound to GFP reporter) (Kiehart et al., 2000) or the Cherry fluorescent equivalent,
421 sChMCA (Abreu-Blanco et al., 2011a), was used to follow wound repair dynamics of the cortical
422 cytoskeleton.

423 *wimp* (*RpL140*^{wimp}) reduces maternal gene expression of a specific subset of genes in the
424 early *Drosophila* embryo (Liu et al., 2009; Parkhurst and Ish-Horowicz, 1991; Verboon et al.,
425 2018). Reduced *chickadee* embryos were obtained from trans-heterozygous females generated
426 by crossing *chickadee*^{221} to *RpL140*^{wimp}.

427 We attempted InR knockdown in three ways: 1) expressing one shRNA (GL00139) using one
428 maternal-GAL4 driver (BDSC #7063), 2) expressing two shRNAs (HMS03166 and GL00139)
429 using one maternal-GAL4 driver (BDSC #70637063), and 3) expressing one shRNA (GL00139)
430 using one maternal-GAL4 (BDSC #7063) in an *InR*^{05545} heterozygous mutant backgrounds. We
431 achieved only 50% knockdown with approach (1), and no eggs were produced by approach (3).
432 We achieved 87% knockdown with approach (2) and this condition was used for the phenotypic
433 analyses included here.

434 For the MS2-MCP system (Forrest and Gavis, 2003; Weil et al., 2006), female virgins
435 maternally expressing MCP-GFP and Histone-RFP were crossed with males expressing 24xMS2
436 stem loops and lacZ driven by hunchback P2 enhancer and promoter. F1 embryos (MCP-GFP,
437 Histone-RFP/+; 24xMS2-lacZ/+) at NC9-10 stages were used for imaging where the 24xMS2-
438 lacZ mRNA is contributed zygotically.

439 Localization patterns and mutant analyses were performed at least twice from independent
440 genetic crosses and ≥10 embryos were examined unless otherwise noted. Images representing
441 the average phenotype were selected for figures.

442

443 **Quantification of mRNA levels in RNAi mutants**

444 To harvest total RNA, 100-150 embryos were collected after a 30 min incubation at 25°C, treated
445 with TRIzol (Invitrogen/Thermo Fisher Scientific) and then with DNase I (Sigma). 1 µg of total
446 RNA and oligo (dT) primers were reverse transcribed using the iScript gDNA Clear cDNA
447 Synthesis Kit (Bio-Rad). RT-PCR was performed using the iTaq Universal SYBR Green Supermix
448 (Bio-Rad) and primers obtained from the Fly Primer Bank listed on Table S2B. We were unable
449 to identify primer sets that would work for qPCR for Geko, Ama, l(3)neo38, danr, and CG4960.

450 Each gene in question was derived from two individual parent sets and run in two technical
451 replicates on the CFX96TM Real Time PCR Detection System (Bio-Rad) for a total of four
452 samples per gene. RpL32 (RP-49) or GAPDH were used as reference genes and the knockdown
453 efficency (%) was obtained using the ΔΔCq calculation method compared to the control (GAL4
454 only).

455

456 **Embryo handling and preparation**

457 NC4-6 embryos were collected for 30 min at 25°C, then harvested at room temperature (22°C).
458 Collected embryos were dechorionated by hand, desiccated for 5 min, mounted onto No. 1.5
459 coverslips coated with glue, and covered with Series 700 halocarbon oil (Halocarbon Products
460 Corp.) as previously described (Abreu-Blanco et al., 2011a).

461

462 **Drug Injections**

463 Pharmacological inhibitors were injected into NC4-6 staged *Drosophila* embryos, incubated at
464 room temperature (22°C) for 5 min, and then subjected to laser wounding. The following inhibitors
465 were used: α-amanitin (1 mg/ml; Sigma-Aldrich); puromycin (10 mg/ml; Sigma-Aldrich). The
466 inhibitors were prepared in injection buffer (5 mM KCl, 0.1 mM NaP pH6.8). Injection buffer alone
467 was used as the control.

468

469 **Laser Wounding**

470 All wounds were generated with a pulsed nitrogen N2 micropoint laser (Andor Technology Ltd.)
471 set to 435nm and focused at the lateral surface of the embryo. A circular targeted region of
472 16x15.5 µm was selected along the lateral midsection of the embryo, and ablation was controlled
473 by MetaMorph software (Molecular Devices). Average ablation time was less than 3 seconds and
474 time-lapse image acquisition was initiated immediately after ablation. Upon ablation, a grid-like
475 pattern is sometimes observed (fluorescent dots within the wound area), as a result of the laser
476 scoring the vitelline membrane that envelops the embryo. This vitelline membrane scoring has no

477 effect on wound repair dynamics.

478

479 **Immunostaining of wounded embryos**

480 Embryos (1-2 min post-wounding) were fixed in formaldehyde saturated heptane for 40 min. The
481 vitelline membrane was removed by hand and the embryos were then washed 3 times with PAT
482 [1x PBS, 0.1% Tween-20, 1% bovine serum albumin (BSA), 0.05% azide], then blocked in PAT
483 for 2h at 4°C. Embryos were incubated with mouse anti-chickadee antibody (chi 1J; 1:10;
484 Developmental Studies Hybridoma Bank) and guinea pig anti-Girdin antibody (1:500; provided by
485 Patrick Laprise) (Houssin et al., 2015) and for 24h at 4°C. Embryos were then washed 3 times
486 with XNS (1x PBS, 0.1% Tween-20, 0.1% BSA, 4% normal goat serum) for 40 min each. Embryos
487 were incubated with Alexa Fluor 568- and Alexa Fluor 633- conjugated secondary antibodies
488 (1:1000; Invitrogen) overnight at 4°C. Embryos were washed with PTW (1x PBS, 0.1% Tween-
489 20), incubated with Alexa Fluor 488-conjugated Phalloidin at 0.005 units/µl (Molecular
490 Probes/Invitrogen, Rockford, IL) at room temperature for 1 h, washed with PTW, and then imaged.

491

492 **Live Image Acquisition**

493 All imaging was done using a Revolution WD systems (Andor Technology Ltd.) mounted on a
494 Leica DMi8 (Leica Microsystems Inc.) with a 63x/1.4 NA objective lens under the control of
495 MetaMorph software (Molecular devices). Images were acquired using a 488 nm, 561 nm, and
496 633 nm Lasers and Andor iXon Ultra 897 EMCCD camera (Andor Technology Ltd.). All time-lapse
497 images were acquired with 17-20 µm stacks/0.25 µm steps. For single color, images were
498 acquired every 30 sec for 15 min and then every 60 sec for 25 min. For dual green and red colors,
499 images were acquired every 45 sec for 30-40 min.

500

501 **Image processing and analysis**

502 Image processing was performed using FIJI software (Schindelin et al., 2012). Kymographs were
503 generated using the crop feature to select ROIs of 5.3 x 94.9 µm. To generate fluorescent profile
504 plots by R, 10 pixel sections across the wound from a single embryo were generated using Fiji as
505 we described previously (Nakamura et al., 2017). The lines represent the averaged fluorescent
506 intensity and gray area is the 95% confidence interval. Line profiles from the left to right
507 correspond to the top to bottom of the images unless otherwise noted. Wound area was manually
508 measured using Fiji and the values were imported into Prism 8.2.1 (GraphPad Software Inc.) to
509 construct corresponding graphs. Figures were assembled in Canvas Draw 6 for Mac (Canvas
510 GFX, Inc.).

Microarray Preparation and Processing

Expression profiles were obtained using the FHCRC Fly 12k spotted array (GEO platform, GPL 1908). Embryos, prepared for wounding, were either wounded 8 times or left unwounded, then collected for total RNA extraction. Sample labeling and hybridization protocols were performed as described by Fazzio et al (Fazzio et al., 2001). Specifically, cDNA targets were generated from total RNA using a standard amino-allyl labelling protocol where 30 ug of total RNA from each wounding condition (wounded vs non-wounded) were coupled to either Cy3 or Cy5 fluorophores. Targets were co-hybridized to microarrays for 16 hours at 63C and sequentially washed at room temperature (22C) in: 1 x SSC and 0.03% SDS for 2 mins, 1 x SSC for 2 mins, 0.2 x SSC with agitation for 20 mins, and 0.05 x SSC with agitation for 10 mins. Arrays were immediately centrifuged until dry and scanned using a GenePix 4000B scanner (Molecular Devices, Sunnyvale, CA). Image analysis was performed using GenePix Pro 6.0.

Microarray Analysis

Wounded and non-wounded samples were independently replicated 4 times each at the 0 min and 30 min time point. For each array, spot intensity signals were filtered and removed if the values did not exceed 3 standard deviations above the background signal, if the background subtracted signal was <100 in both channels, or if a spot was flagged as questionable by the GenePix Pro Software. Spot-levels ratios were $\log_2$ transformed and loess normalized using the Bioconductor package *limma(Smyth et al., 2005)*. Differential gene expression between wounded and non-wounded states was determined using the Bioconductor package *limma,* and a false discovery rate (FDR) method was used to correct for multiple testing (Reiner et al., 2003). Significant differential gene expression was defined as $|\log_2 (\text{ratio})| \geq 0.585$ ($\pm$ 1.5-fold) with FDR set to 5%. Gene ontology enrichment scores were determined using DAVID with significance based on EASE scores corrected for multiple testing (Huang da et al., 2009a, b). The microarray datasets are available at GEO (NCBI Gene Expression Omnibus) under accession numbers: GSE39481, GSE39482, and GSE39483.

TAD analysis

Genes were mapped to previously described TADs (Li et al., 2017). A TAD by up/down regulated gene versus unaffected gene expressed on the microarray contigency table was assembled. Fisher's exact test of independence was used to test the null hypothesis that porportion of differentially expressed genes was different per TAD.

545

546 **Gene Size Analysis**

547 Gene size was determined as the size of the largest expressed transcript per gene (dm6 build)
548 expressed on the arrays. The median plus 95% CI was determined using the bootstrap procedure
549 and 1000 iterations.

550

Acknowledgements

We thank Ryan Basom, Patrick Laprise, Scott Somers, the Bloomington Stock Center, the Kyoto Stock Center, the Harvard Transgenic RNAi Project, the Vienna Drosophila RNAi Center, the Drosophila Genomics Resource Center, and the Developmental Studies Hybridoma Bank for advice, antibodies, DNAs, flies, and other reagents used in this study. This research was supported by NIH GM111635 (to SMP) and NCI Cancer Center Support Grant P30 CA015704 (for Shared Resources).

Author Contributions

All authors contributed to the design of the experiments, performed experiments, and analyzed data. JJD and JMV performed the bioinformatic analyses. MN, ANMD, JMV, and SMP wrote the manuscript with input from all authors.

Competing Interests

The authors declare no competing or financial interests.

References

Abreu-Blanco, M.T., Verboon, J.M., and Parkhurst, S.M. (2011a). Cell wound repair in Drosophila occurs through three distinct phases of membrane and cytoskeletal remodeling. The Journal of cell biology *193*, 455-464.

Abreu-Blanco, M.T., Verboon, J.M., and Parkhurst, S.M. (2011b). Single cell wound repair: Dealing with life's little traumas. Bioarchitecture *1*, 114-121.

Abreu-Blanco, M.T., Verboon, J.M., and Parkhurst, S.M. (2014). Coordination of Rho family GTPase activities to orchestrate cytoskeleton responses during cell wound repair. Current biology : CB *24*, 144-155.

Amoyel, M., Hillion, K.H., Margolis, S.R., and Bach, E.A. (2016). Somatic stem cell differentiation is regulated by PI3K/Tor signaling in response to local cues. Development *143*, 3914-3925.

Andrews, N.W., and Corrotte, M. (2018). Plasma membrane repair. Current biology : CB *28*, R392-R397.

Ardehali, M.B., Yao, J., Adelman, K., Fuda, N.J., Petesch, S.J., Webb, W.W., and Lis, J.T. (2009). Spt6 enhances the elongation rate of RNA polymerase II in vivo. The EMBO journal *28*, 1067-1077.

Artieri, C.G., and Fraser, H.B. (2014). Transcript length mediates developmental timing of gene expression across Drosophila. Mol Biol Evol *31*, 2879-2889.

Bement, W.M., Mandato, C.A., and Kirsch, M.N. (1999). Wound-induced assembly and closure of an actomyosin purse string in Xenopus oocytes. Current biology : CB *9*, 579-587.

Bement, W.M., Yu, H.Y., Burkel, B.M., Vaughan, E.M., and Clark, A.G. (2007). Rehabilitation and the single cell. Current opinion in cell biology *19*, 95-100.

Benink, H.A., and Bement, W.M. (2005). Concentric zones of active RhoA and Cdc42 around single cell wounds. The Journal of cell biology *168*, 429-439.

Bi, G.Q., Alderton, J.M., and Steinhardt, R.A. (1995). Calcium-regulated exocytosis is required for cell membrane resealing. The Journal of cell biology *131*, 1747-1758.

Brand, A.H., and Perrimon, N. (1993). Targeted gene expression as a means of altering cell fates and generating dominant phenotypes. Development *118*, 401-415.

Brem, H., and Tomic-Canic, M. (2007). Cellular and molecular basis of wound healing in diabetes. J Clin Invest *117*, 1219-1222.

Britton, J.S., Lockwood, W.K., Li, L., Cohen, S.M., and Edgar, B.A. (2002). Drosophila's insulin/PI3-kinase pathway coordinates cellular metabolism with nutritional conditions. Developmental cell *2*, 239-249.

Brunet, A., Bonni, A., Zigmond, M.J., Lin, M.Z., Juo, P., Hu, L.S., Anderson, M.J., Arden, K.C., Blenis, J., and Greenberg, M.E. (1999). Akt promotes cell survival by phosphorylating and inhibiting a Forkhead transcription factor. Cell *96*, 857-868.

Burkel, B.M., Benink, H.A., Vaughan, E.M., von Dassow, G., and Bement, W.M. (2012). A Rho GTPase signal treadmill backs a contractile array. Developmental cell *23*, 384-396.

Choi, J.S., Kim, K.H., Oh, E., Shin, Y.K., Seo, J., Kim, S.H., Park, S., and Choi, Y.L. (2017). Girdin protein expression is associated with poor prognosis in patients with invasive breast cancer. Pathology *49*, 618-626.

610 Clarke, M.S., Caldwell, R.W., Chiao, H., Miyake, K., and McNeil, P.L. (1995). Contraction-
611 induced cell wounding and release of fibroblast growth factor in heart. Circ Res *76*, 927-934.

612 Cooper, S.T., and McNeil, P.L. (2015). Membrane Repair: Mechanisms and Pathophysiology.
613 Physiol Rev *95*, 1205-1240.

614 Coulombe, P.A., Hutton, M.E., Letai, A., Hebert, A., Paller, A.S., and Fuchs, E. (1991). Point
615 mutations in human keratin 14 genes of epidermolysis bullosa simplex patients: genetic and
616 functional analyses. Cell *66*, 1301-1311.

617 Draeger, A., Schoenauer, R., Atanassoff, A.P., Wolfmeier, H., and Babiychuk, E.B. (2014).
618 Dealing with damage: plasma membrane repair mechanisms. Biochimie *107 Pt A*, 66-72.

619 Fazzio, T.G., Kooperberg, C., Goldmark, J.P., Neal, C., Basom, R., Delrow, J., and Tsukiyama,
620 T. (2001). Widespread collaboration of Isw2 and Sin3-Rpd3 chromatin remodeling complexes in
621 transcriptional repression. Molecular and cellular biology *21*, 6450-6460.

622 Fein, A., and Terasaki, M. (2005). Rapid increase in plasma membrane chloride permeability
623 during wound resealing in starfish oocytes. J Gen Physiol *126*, 151-159.

624 Figueroa-Clarevega, A., and Bilder, D. (2015). Malignant Drosophila tumors interrupt insulin
625 signaling to induce cachexia-like wasting. Developmental cell *33*, 47-55.

626 Foe, V.E., and Alberts, B.M. (1983). Studies of nuclear and cytoplasmic behaviour during the
627 five mitotic cycles that precede gastrulation in Drosophila embryogenesis. Journal of cell
628 science *61*, 31-70.

629 Forrest, K.M., and Gavis, E.R. (2003). Live imaging of endogenous RNA reveals a diffusion and
630 entrapment mechanism for nanos mRNA localization in Drosophila. Current biology : CB *13*,
631 1159-1168.

632 Fukaya, T., Lim, B., and Levine, M. (2017). Rapid Rates of Pol II Elongation in the Drosophila
633 Embryo. Current biology : CB *27*, 1387-1391.

634 Galan, J.E., and Bliska, J.B. (1996). Cross-talk between bacterial pathogens and their host
635 cells. Annu Rev Cell Dev Biol *12*, 221-255.

636 Galiano, R.D., Tepper, O.M., Pelo, C.R., Bhatt, K.A., Callaghan, M., Bastidas, N., Bunting, S.,
637 Steinmetz, H.G., and Gurtner, G.C. (2004). Topical vascular endothelial growth factor
638 accelerates diabetic wound healing through increased angiogenesis and by mobilizing and
639 recruiting bone marrow-derived cells. Am J Pathol *164*, 1935-1947.

640 Garcia, H.G., Tikhonov, M., Lin, A., and Gregor, T. (2013). Quantitative imaging of transcription
641 in living Drosophila embryos links polymerase activity to patterning. Current biology : CB *23*,
642 2140-2145.

643 Ghiglione, C., Jouandin, P., Cerezo, D., and Noselli, S. (2018). The Drosophila insulin pathway
644 controls Profilin expression and dynamic actin-rich protrusions during collective cell migration.
645 Development *145*.

646 Giuliani, F., Giuliani, G., Bauer, R., and Rabouille, C. (2013). Innexin 3, a new gene required for
647 dorsal closure in Drosophila embryo. PloS one *8*, e69212.

648 Grembowicz, K.P., Sprague, D., and McNeil, P.L. (1999). Temporary disruption of the plasma
649 membrane is required for c-fos expression in response to mechanical stress. Molecular biology
650 of the cell *10*, 1247-1257.

651 Gurtner, G.C., Werner, S., Barrandon, Y., and Longaker, M.T. (2008). Wound repair and
652 regeneration. Nature *453*, 314-321.

Haeusler, R.A., McGraw, T.E., and Accili, D. (2018). Biochemical and cellular properties of insulin receptor signalling. Nature reviews Molecular cell biology *19*, 31-44.

Hartung, A., Ordelheide, A.M., Staiger, H., Melzer, M., Haring, H.U., and Lammers, R. (2013). The Akt substrate Girdin is a regulator of insulin signaling in myoblast cells. Biochimica et biophysica acta *1833*, 2803-2811.

Hoskins, R.A., Landolin, J.M., Brown, J.B., Sandler, J.E., Takahashi, H., Lassmann, T., Yu, C., Booth, B.W., Zhang, D., Wan, K.H.*, et al.* (2011). Genome-wide analysis of promoter architecture in Drosophila melanogaster. Genome research *21*, 182-192.

Houssin, E., Tepass, U., and Laprise, P. (2015). Girdin-mediated interactions between cadherin and the actin cytoskeleton are required for epithelial morphogenesis in Drosophila. Development *142*, 1777-1784.

Huang da, W., Sherman, B.T., and Lempicki, R.A. (2009a). Bioinformatics enrichment tools: paths toward the comprehensive functional analysis of large gene lists. Nucleic acids research *37*, 1-13.

Huang da, W., Sherman, B.T., and Lempicki, R.A. (2009b). Systematic and integrative analysis of large gene lists using DAVID bioinformatics resources. Nature protocols *4*, 44-57.

Joost, S., Jacob, T., Sun, X., Annusver, K., La Manno, G., Sur, I., and Kasper, M. (2018). Single-Cell Transcriptomics of Traced Epidermal and Hair Follicle Stem Cells Reveals Rapid Adaptations during Wound Healing. Cell reports *25*, 585-597 e587.

Kakanj, P., Moussian, B., Gronke, S., Bustos, V., Eming, S.A., Partridge, L., and Leptin, M. (2016). Insulin and TOR signal in parallel through FOXO and S6K to promote epithelial wound healing. Nature communications *7*, 12972.

Kiehart, D.P., Galbraith, C.G., Edwards, K.A., Rickoll, W.L., and Montague, R.A. (2000). Multiple forces contribute to cell sheet morphogenesis for dorsal closure in Drosophila. The Journal of cell biology *149*, 471-490.

Kono, K., Saeki, Y., Yoshida, S., Tanaka, K., and Pellman, D. (2012). Proteasomal degradation resolves competition between cell polarization and cellular wound healing. Cell *150*, 151-164.

Kushnir, T., Mezuman, S., Bar-Cohen, S., Lange, R., Paroush, Z., and Helman, A. (2017). Novel interplay between JNK and Egfr signaling in Drosophila dorsal closure. PLoS genetics *13*, e1006860.

Kwon, Y., Song, W., Droujinine, I.A., Hu, Y., Asara, J.M., and Perrimon, N. (2015). Systemic organ wasting induced by localized expression of the secreted insulin/IGF antagonist ImpL2. Developmental cell *33*, 36-46.

Lautemann, J., and Bohrmann, J. (2016). Relating proton pumps with gap junctions: colocalization of ductin, the channel-forming subunit c of V-ATPase, with subunit a and with innexins 2 and 3 during Drosophila oogenesis. BMC Dev Biol *16*, 24.

Lee, K., Kim, J., Kohler, M., Yu, J., Shi, Y., Yang, S.N., Ryu, S.H., and Berggren, P.O. (2018). Blocking Ca(2+) Channel beta3 Subunit Reverses Diabetes. Cell reports *24*, 922-934.

Li, Q., Tjong, H., Li, X., Gong, K., Zhou, X.J., Chiolo, I., and Alber, F. (2017). The three-dimensional genome organization of Drosophila melanogaster through data integration. Genome biology *18*, 145.

Li, Y., Fetchko, M., Lai, Z.C., and Baker, N.E. (2003). Scabrous and Gp150 are endosomal proteins that regulate Notch activity. Development *130*, 2819-2827.

Liu, R., Abreu-Blanco, M.T., Barry, K.C., Linardopoulou, E.V., Osborn, G.E., and Parkhurst, S.M. (2009). Wash functions downstream of Rho and links linear and branched actin nucleation factors. Development *136*, 2849-2860.

Lopez-Sanchez, I., Ma, G.S., Pedram, S., Kalogriopoulos, N., and Ghosh, P. (2015). GIV/girdin binds exocyst subunit-Exo70 and regulates exocytosis of GLUT4 storage vesicles. Biochem Biophys Res Commun *468*, 287-293.

Manzano-Nunez, F., Arambul-Anthony, M.J., Galan Albinana, A., Leal Tassias, A., Acosta Umanzor, C., Borreda Gasco, I., Herrera, A., Forteza Vila, J., Burks, D.J., and Noon, L.A. (2019). Insulin resistance disrupts epithelial repair and niche-progenitor Fgf signaling during chronic liver injury. PLoS biology *17*, e2006972.

Martin, P., and Nobes, C.D. (1992). An early molecular component of the wound healing response in rat embryos--induction of c-fos protein in cells at the epidermal wound margin. Mech Dev *38*, 209-215.

Martino, F., Perestrelo, A.R., Vinarsky, V., Pagliari, S., and Forte, G. (2018). Cellular Mechanotransduction: From Tension to Function. Front Physiol *9*, 824.

McNeil, P.L., and Kirchhausen, T. (2005). An emergency response team for membrane repair. Nature reviews Molecular cell biology *6*, 499-505.

McNeil, P.L., and Terasaki, M. (2001). Coping with the inevitable: how cells repair a torn surface membrane. Nature cell biology *3*, E124-129.

Miyake, K., and McNeil, P.L. (1995). Vesicle accumulation and exocytosis at sites of plasma membrane disruption. The Journal of cell biology *131*, 1737-1745.

Moe, A.M., Golding, A.E., and Bement, W.M. (2015). Cell healing: Calcium, repair and regeneration. Seminars in cell & developmental biology *45*, 18-23.

Nakamura, F., Stossel, T.P., and Hartwig, J.H. (2011). The filamins: organizers of cell structure and function. Cell Adh Migr *5*, 160-169.

Nakamura, M., Dominguez, A.N.M., Decker, J.R., Hull, A.J., Verboon, J.M., and Parkhurst, S.M. (2018). Into the breach: how cells cope with wounds. Open Biol *8*.

Nakamura, M., Verboon, J.M., and Parkhurst, S.M. (2017). Prepatterning by RhoGEFs governs Rho GTPase spatiotemporal dynamics during wound repair. The Journal of cell biology *216*, 3959-3969.

O'Farrell, P.H. (1992). Developmental biology. Big genes and little genes and deadlines for transcription. Nature *359*, 366-367.

Parkhurst, S.M., and Ish-Horowicz, D. (1991). wimp, a dominant maternal-effect mutation, reduces transcription of a specific subset of segmentation genes in Drosophila. Genes & development *5*, 341-357.

Petrof, B.J., Shrager, J.B., Stedman, H.H., Kelly, A.M., and Sweeney, H.L. (1993). Dystrophin protects the sarcolemma from stresses developed during muscle contraction. Proceedings of the National Academy of Sciences of the United States of America *90*, 3710-3714.

Puig, O., and Tjian, R. (2005). Transcriptional feedback control of insulin receptor by dFOXO/FOXO1. Genes & development *19*, 2435-2446.

Rameh, L.E., and Cantley, L.C. (1999). The role of phosphoinositide 3-kinase lipid products in cell function. The Journal of biological chemistry *274*, 8347-8350.

Reiner, A., Yekutieli, D., and Benjamini, Y. (2003). Identifying differentially expressed genes using false discovery rate controlling procedures. Bioinformatics *19*, 368-375.

Rorth, P. (1998). Gal4 in the Drosophila female germline. Mech Dev *78*, 113-118.

Rutter, G.A., Tsuboi, T., and Ravier, M.A. (2006). Ca2+ microdomains and the control of insulin secretion. Cell Calcium *40*, 539-551.

Sandler, J.E., Irizarry, J., Stepanik, V., Dunipace, L., Amrhein, H., and Stathopoulos, A. (2018). A Developmental Program Truncates Long Transcripts to Temporally Regulate Cell Signaling. Developmental cell *47*, 773-784 e776.

Schindelin, J., Arganda-Carreras, I., Frise, E., Kaynig, V., Longair, M., Pietzsch, T., Preibisch, S., Rueden, C., Saalfeld, S., Schmid, B.*, et al.* (2012). Fiji: an open-source platform for biological-image analysis. Nature methods *9*, 676-682.

Shaulian, E., and Karin, M. (2002). AP-1 as a regulator of cell life and death. Nature cell biology *4*, E131-136.

Shermoen, A.W., and O'Farrell, P.H. (1991). Progression of the cell cycle through mitosis leads to abortion of nascent transcripts. Cell *67*, 303-310.

Smyth, G.K., Michaud, J., and Scott, H.S. (2005). Use of within-array replicate spots for assessing differential expression in microarray experiments. Bioinformatics *21*, 2067-2075.

Sokac, A.M., and Wieschaus, E. (2008a). Local actin-dependent endocytosis is zygotically controlled to initiate Drosophila cellularization. Developmental cell *14*, 775-786.

Sokac, A.M., and Wieschaus, E. (2008b). Zygotically controlled F-actin establishes cortical compartments to stabilize furrows during Drosophila cellularization. Journal of cell science *121*, 1815-1824.

Sonnemann, K.J., and Bement, W.M. (2011). Wound repair: toward understanding and integration of single-cell and multicellular wound responses. Annu Rev Cell Dev Biol *27*, 237-263.

Steinhardt, R.A., Bi, G., and Alderton, J.M. (1994). Cell membrane resealing by a vesicular mechanism similar to neurotransmitter release. Science *263*, 390-393.

Tang, S.K.Y., and Marshall, W.F. (2017). Self-repairing cells: How single cells heal membrane ruptures and restore lost structures. Science *356*, 1022-1025.

Teleman, A.A., Chen, Y.W., and Cohen, S.M. (2005). 4E-BP functions as a metabolic brake used under stress conditions but not during normal growth. Genes & development *19*, 1844-1848.

Terasaki, M., Miyake, K., and McNeil, P.L. (1997). Large plasma membrane disruptions are rapidly resealed by Ca2+-dependent vesicle-vesicle fusion events. The Journal of cell biology *139*, 63-74.

Thummel, C.S., Burtis, K.C., and Hogness, D.S. (1990). Spatial and temporal patterns of E74 transcription during Drosophila development. Cell *61*, 101-111.

Togo, T. (2004). Long-term potentiation of wound-induced exocytosis and plasma membrane repair is dependent on cAMP-response element-mediated transcription via a protein kinase C- and p38 MAPK-dependent pathway. The Journal of biological chemistry *279*, 44996-45003.

Toshniwal, A.G., Gupta, S., Mandal, L., and Mandal, S. (2019). ROS Inhibits Cell Growth by Regulating 4EBP and S6K, Independent of TOR, during Development. Developmental cell *49*, 473-489 e479.

Vastenhouw, N.L., Cao, W.X., and Lipshitz, H.D. (2019). The maternal-to-zygotic transition revisited. Development *146*.

Velnar, T., Bailey, T., and Smrkolj, V. (2009). The wound healing process: an overview of the cellular and molecular mechanisms. J Int Med Res *37*, 1528-1542.

Verboon, J.M., Decker, J.R., Nakamura, M., and Parkhurst, S.M. (2018). Wash exhibits context-dependent phenotypes and, along with the WASH regulatory complex, regulates Drosophila oogenesis. Journal of cell science *131*.

Verboon, J.M., and Parkhurst, S.M. (2015). Rho family GTPases bring a familiar ring to cell wound repair. Small GTPases *6*, 1-7.

Verrier, B., Muller, D., Bravo, R., and Muller, R. (1986). Wounding a fibroblast monolayer results in the rapid induction of the c-fos proto-oncogene. The EMBO journal *5*, 913-917.

Vinayagam, A., Kulkarni, M.M., Sopko, R., Sun, X., Hu, Y., Nand, A., Villalta, C., Moghimi, A., Yang, X., Mohr, S.E.*, et al.* (2016). An Integrative Analysis of the InR/PI3K/Akt Network Identifies the Dynamic Response to Insulin Signaling. Cell reports *16*, 3062-3074.

Wang, S., Lei, Y., Cai, Z., Ye, X., Li, L., Luo, X., and Yu, C. (2018a). Girdin regulates the proliferation and apoptosis of pancreatic cancer cells via the PI3K/Akt signalling pathway. Oncol Rep *40*, 599-608.

Wang, X., Enomoto, A., Weng, L., Mizutani, Y., Abudureyimu, S., Esaki, N., Tsuyuki, Y., Chen, C., Mii, S., Asai, N.*, et al.* (2018b). Girdin/GIV regulates collective cancer cell migration by controlling cell adhesion and cytoskeletal organization. Cancer Sci *109*, 3643-3656.

Weil, T.T., Forrest, K.M., and Gavis, E.R. (2006). Localization of bicoid mRNA in late oocytes is maintained by continual active transport. Developmental cell *11*, 251-262.

Yao, J., Ardehali, M.B., Fecko, C.J., Webb, W.W., and Lis, J.T. (2007). Intranuclear distribution and local dynamics of RNA polymerase II during transcription activation. Molecular cell *28*, 978-990.

Yates, S., and Rayner, T.E. (2002). Transcription factor activation in response to cutaneous injury: role of AP-1 in reepithelialization. Wound Repair Regen *10*, 5-15.

Yumura, S., Hashima, S., and Muranaka, S. (2014). Myosin II does not contribute to wound repair in Dictyostelium cells. Biol Open *3*, 966-973.

Supplementary Video Legends

Video 1 | Translation and transcription are needed for different aspects of cell wound repair. a-c, Time-lapse confocal xy images from Drosophila NC4-6 staged embryos expressing an actin marker (sGMCA): control (buffer only) (**a**), alpha-amanitin injected (**b**), and puromycin injected (**c**). Time post-wounding is indicated. UW: unwounded.

Video 2 | Knockdown of up-regulated genes results in wound over-expansion and abnormal actin dynamics. a-h, Time-lapse confocal xy images from Drosophila NC4-6 staged embryos expressing an actin marker (sGMCA): control (w^{1118}/+; sGMCA, 7063/+) (**a**), ImpL2^{RNAi}/+; sGMCA, 7063/+ (**b**), EGFR^{RNAi}/+; sGMCA, 7063/+ (**c**), Gp150^{RNAi}/sGMCA, 7063 (**d**), Inx3^{RNAi}/sGMCA, 7063 (**e**), Thor^{RNAi}/sGMCA, 7063 (**f**), Jbug^{RNAi}/sGMCA, 7063 (**g**), Nullo^{RNAi}/sGMCA, 7063 (**h**).). Time post-wounding is indicated. UW: unwounded.

Video 3 | Knockdown of down-regulated genes results in wound over-expansion and abnormal actin dynamics. a-g, Time-lapse confocal xy images from Drosophila NC4-6 staged embryos expressing an actin marker (sGMCA): CG31075^{RNAi}/+; sGMCA, 7063/+ (**a**), GstD1^{RNAi}/+; sGMCA, 7063/+ (**b**), dhd^{RNAi}/+; sGMCA, 7063/+ (**c**), Exu^{RNAi}/+; sGMCA, 7063/+ (**d**), CG4960^{RNAi}/+; sGMCA, 7063/+ (**e**), GstD2^{RNAi}/+; sGMCA, 7063/+ (**f**), CG1598^{RNAi}/+; sGMCA, 7063/+ (**g**). Time post-wounding is indicated. UW: unwounded.

Video 4 | Actin dynamics of IIS pathway mutants. a-i, Time-lapse confocal xy images from Drosophila NC4-6 staged embryos expressing an actin marker (sGMCA): insulin-like peptide 4^{RNAi} (Ilp4^{RNAi}; **a**), InR$^{RNAi(1)}$/+; InR$^{RNAi(2)}$/sGMCA, 7063 (**b**), Chico^{RNAi}/sGMCA, 7063 (**c**), Pi3K21B^{RNAi}/sGMCA, 7063 (**d**), Akt1^{RNAi}/sGMCA, 7063 (**e**), FoxO^{RNAi}/sGMCA, 7063 (**f**), Reptor^{RNAi}/sGMCA, 7063 (**g**), Girdin^{RNAi}/+; sGMCA, 7063/+ (**h**), and sGMCA; *chickadee*^{221}/+ sGMCA, *wimp*/+ (reduced chickadee) (**f**). Time post-wounding is indicated. UW: unwounded.

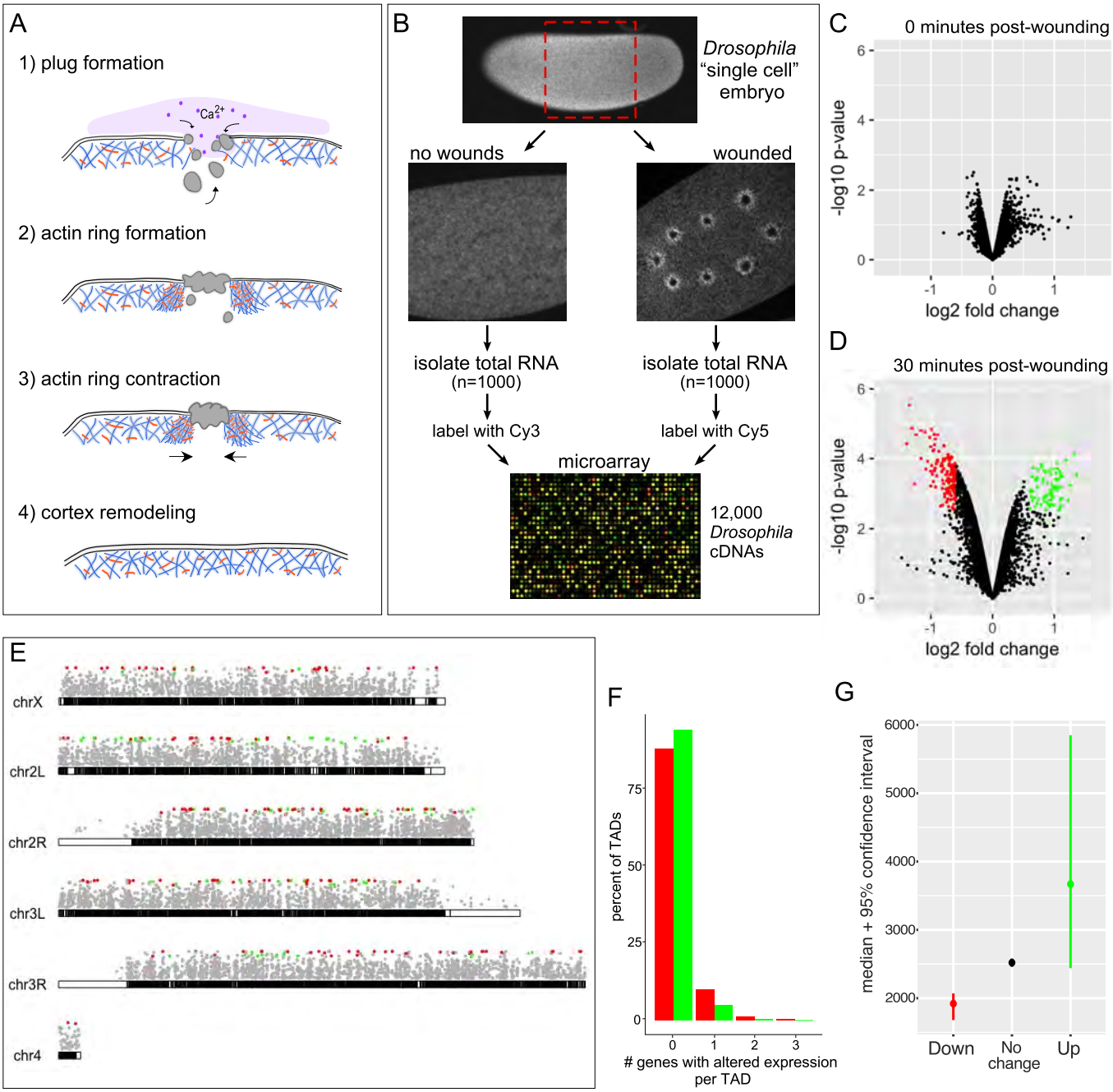

Figure 1. Analysis of differential gene expression following wounding in the *Drosophila* cell wound repair model. (**A**) Schematic of the four major phases of cell wound repair. (**B**) Flow chart depicting the steps involved in microarray processing for examining the transcriptional response to cell wound repair. These analyses were performed for two-timepoints post laser wounding: immediate (0-5 mpw) and near completion (~30 mpw). (**C-D**) Volcano plots showing the differential gene expression for each of the two timepoints. Each dot represents a cDNA corresponding to its fold-change and p-value. Insignificant hits are de picted in black, whereas up-regulated and down-regulated genes are depicted in green and red, respectively. (**E**) *Drosophila* chromosome maps with each of the 4 chromosomes represented by euchromatic regions in black, heterochromatic regions in white, and with the left and right arms of chromosomes 2 and 3 depicted separately. Dots representing genes hits from the late-period microarray with significant up-regulated genes (green) and down-regulated genes (red) placed at their respective location within the genome. (**F**) Percentage of TADs containing the indicated number of up- or down- regulated genes per TAD. (**G**) Average gene size of significantly expressed genes from the ~30 min time point microarray.

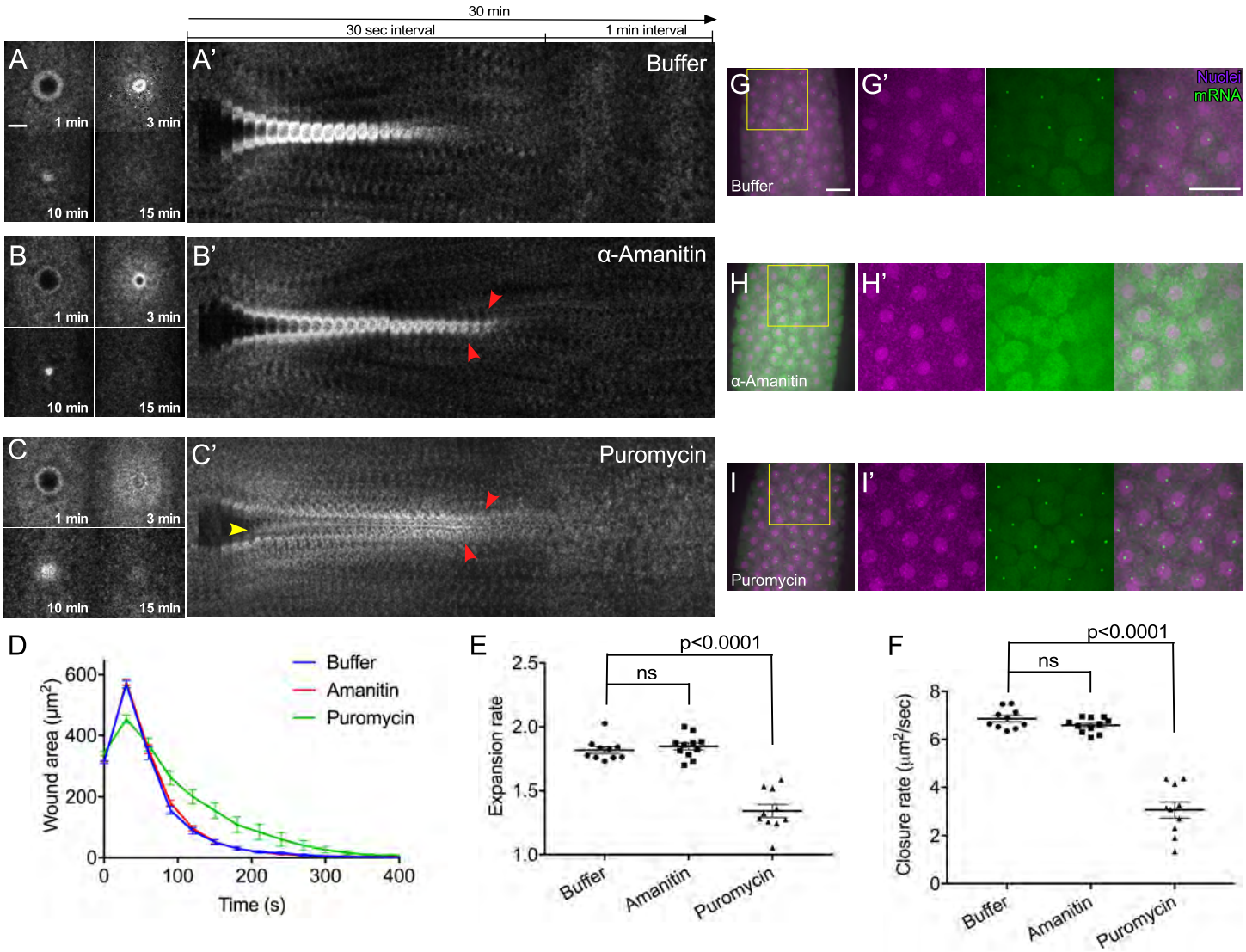

Figure 2. Translation, rather than transcription, is needed for the initiation of cell wound repair . (**A-C**) Confocal projection stills from time-lapse imaging of actin dynamics (sGMCA) during cell wound repair in control (buffer only) (**A**), alpha-amanitin injected (**B**), and puromycin injected (**C**) embryos. (**A'-C'**) XY kymographs across the wound areas depicted in **A-C**, respectively. Note extended actin remodeling (red arrowheads in b',c') and internal actin accumulation (yellow arrowhead in c') (**D**) Quantification of wound area over time for (**A-C'**). Error bars represent ± SEM. (**E-F**) Quantification of wound expansion time (**E**) and wound closure speed (**F**) for conditions indicated. Student's t-test; all p-values indicated. (**G-I**) Confocal projections of a NC 10 embryo expressing the MS2-MCP system injected with: buffer (**G**), alpha-amanitin (**H**), or puromycin (**I**). (**G'-I'**) higher magnification images of the respective regions in (**G-I**) demarcated by the yellow box, showing nuclei (magenta) and nascent mRNA (green). Scale bars: 20 μm.

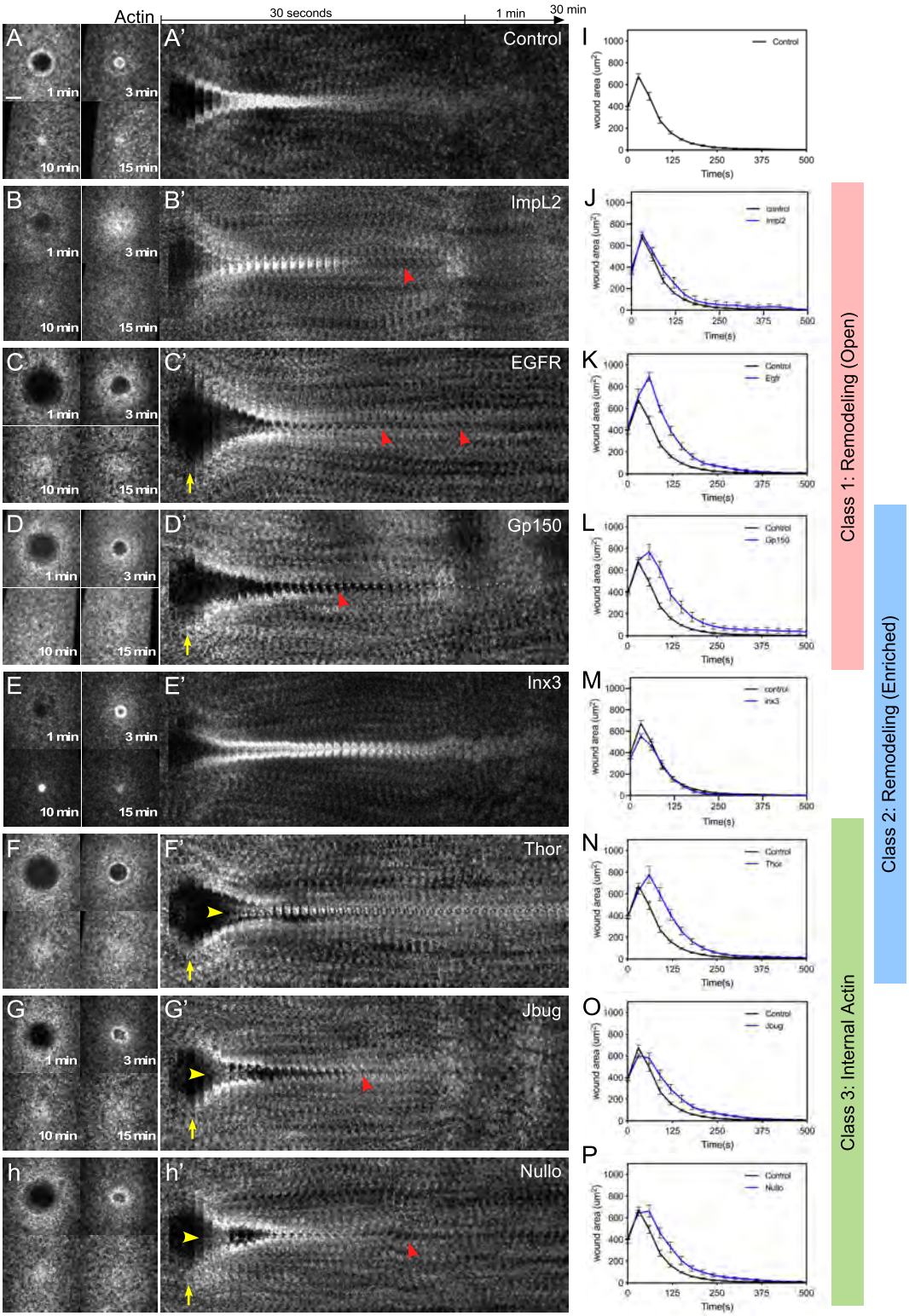

Figure 3. Knockdown of up-regulated genes results in wound over-expansion and abnormal actin dynamics. (**A**-**H**) Confocal XY projections of actin dynamics at 1, 5, 10, and 15 mpw from *Drosophila* NC4-6 embryos coexpressing sGMCA and a UAS-RNAi transgene during cell wound repair for control (w^{1118}/+; sGMCA, 7063/+) (**A**), $ImpL2^{RNAi}$/+; sGMCA, 7063/+ (**B**), $EGFR^{RNAi}$/+; sGMCA, 7063/+ (**C**), $Gp150^{RNAi}$/sGMCA, 7063 (**D**), $Inx3^{RNAi}$/sGMCA, 7063 (**E**), $Thor^{RNAi}$/sGMCA, 7063 (**F**), $Jbug^{RNAi}$/sGMCA, 7063 (**G**), $Nullo^{RNAi}$/sGMCA, 7063 (**H**). (**A'**-**H'**) XY kymographs across the wound areas depicted in (**A**-**H**), respectively. Note wound overexpansion (yellow arrows); internal actin accumulation (yellow arrowhead), and remodeling defect/open wound (red arrowhead). (**I**-**P**) Quantification of wound area over time for (**A**-**H'**), respectively. Error bars represent $\pm$ SEM; n $\geq$ 10. Side bars denote phenotypic classifiers: CLASS 1 (red), CLASS 2 (blue), CLASS 3 (green). Scale bars: 20 μm.

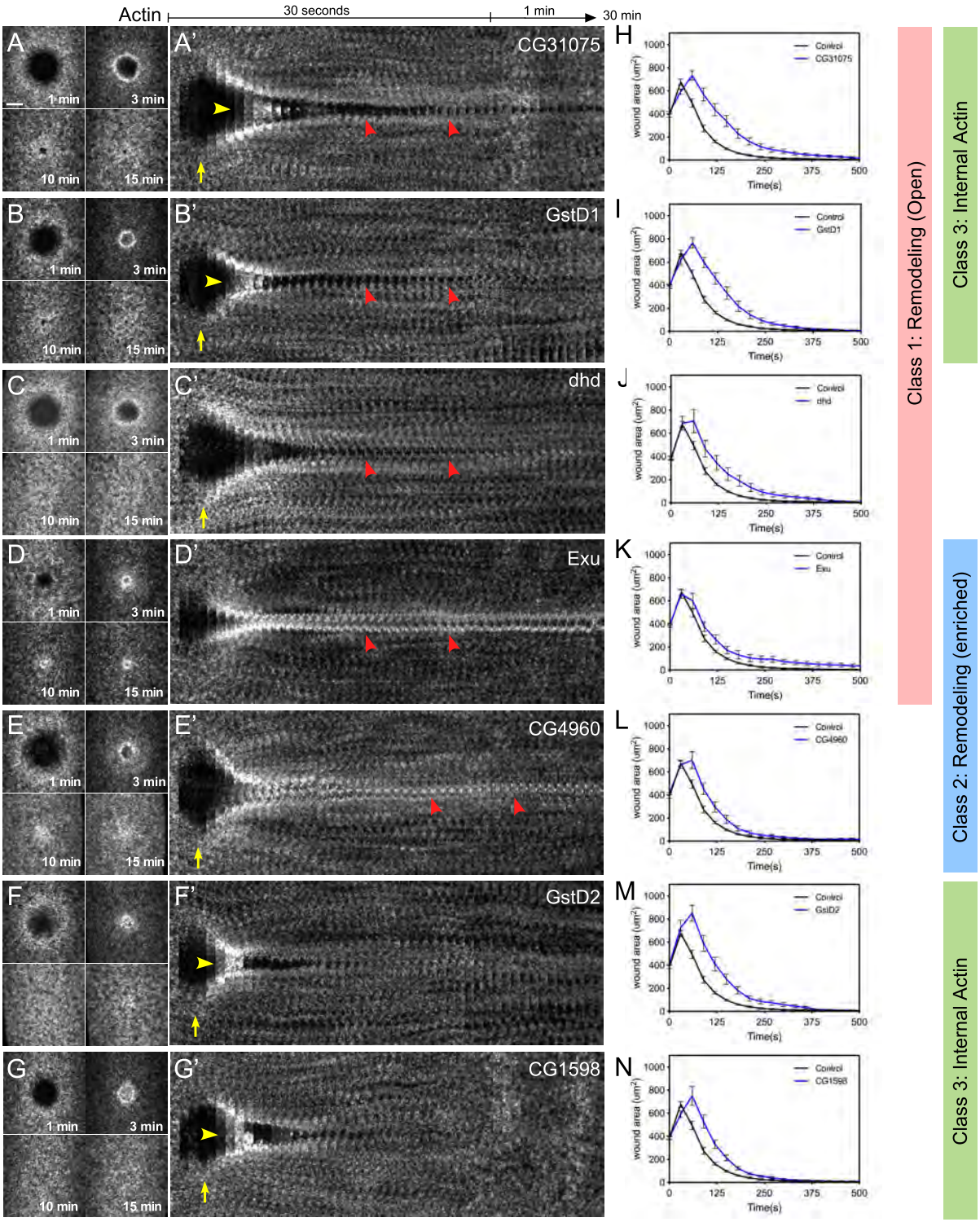

Figure 4. Knockdown of down-regulated genes results in wound over-expansion and abnormal actin dynamics. (**A-G**) Confocal XY projections of actin dynamics at 1, 5, 10, and 15 mpw from *Drosophila* NC4-6 embryos coexpressing sGMCA and a UAS-RNAi transgene during cell wound repair for CG31075^{RNAi}/+; sGMCA, 7063/+ (**A**), GstD1^{RNAi}/+; sGMCA, 7063/+ (**B**), dhd^{RNAi}/+; sGMCA, 7063/+ (**C**), Exu^{RNAi}/+; sGMCA, 7063/+ (**D**), CG4960^{RNAi}/+; sGMCA, 7063/+ (**E**), GstD2^{RNAi}/+; sGMCA, 7063/+ (**F**), CG1598^{RNAi}/+; sGMCA, 7063/+ (**G**). (**A'-G'**) XY kymographs across the wound areas depicted in (**A-G**), respectively. Note wound overexpansion (yellow arrows); internal actin accumulation (yellow arrowhead), and remodeling defect/open wound (red arrowhead). (**H-N**) Quantification of wound area over time for (**A-G'**), respectively. Error bars represent $\pm$ SEM; n $\geq$ 10. Side bars denote phenotypic classifiers: CLASS 1 (red), CLASS 2 (blue), CLASS 3 (green). Scale bars: 20 µm.

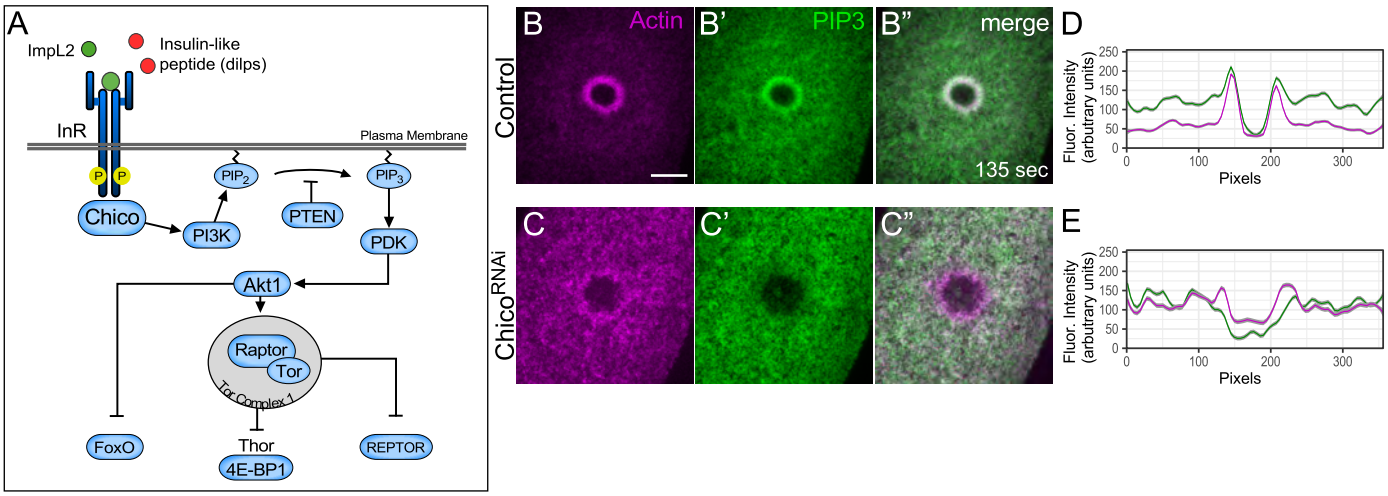

Figure 5. Localization of IIS pathway components. (**A**) Simplified diagram of the IIS pathway in *Drosophila* showing the components tested using GFP reporters and RNAi transgenes. (**B**-**C"**) Confocal xy projection images from *Drosophila* NC4-6 staged embryos co-expressing an actin marker (sChMCA) and GFP-tagged PIP3 in a control (**B**-**B"**) or chico RNAi (**C**-**C"**). (**D-E**) Smoothened fluorescence intensity (arbitrary units) profiles derived from averaged fluorescence intensity values over a 10 pixel width across the wound area in the embryo shown (**B**-**C"**), respectively. Gray area represents the 95% confidence interval. Scale bars: 20 µm.

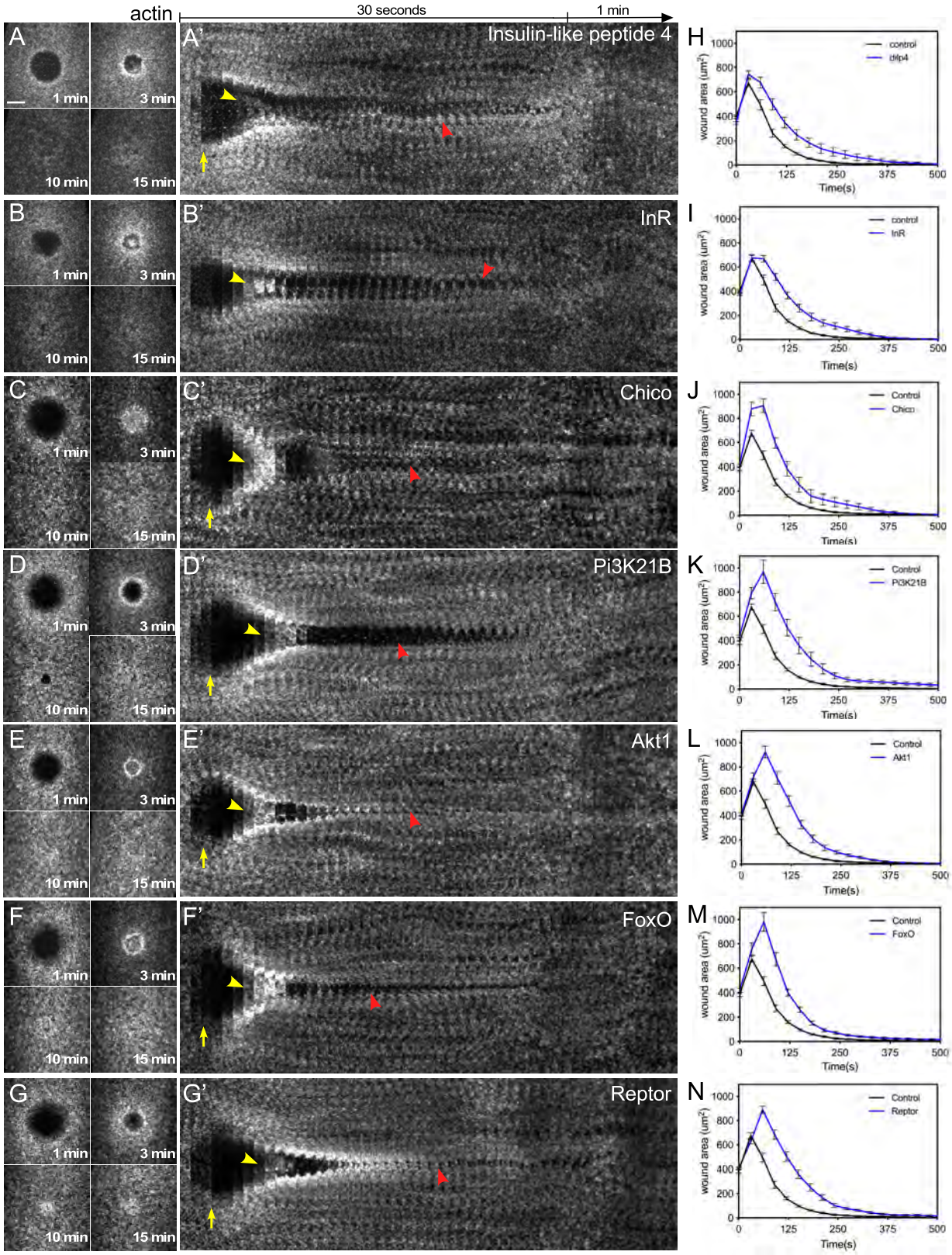

Figure 6. Actin dynamics of IIS pathway mutants. (**A-G**) Confocal XY projections of actin dynamics at 1, 5, 10, and 15 mpw during cell wound repair in *Drosophila* NC4-6 embryos expressing sGMCA and a mutant for insulin-like peptide 4 (*Ilp4*[1]; **A**), or a UAS-RNAi transgene for InR$^{RNAi(1)}$/+; InR$^{RNAi(2)}$/sGMCA, 7063 (**B**), Chico^{RNAi}/sGMCA, 7063 (**C**), Pi3K21B^{RNAi}/sGMCA, 7063 (**D**), Akt1^{RNAi}/sGMCA, 7063 (**E**), FoxO^{RNAi}/sGMCA, 7063 (**F**), and Reptor^{RNAi}/sGMCA, 7063 (**G**). (**A'-G'**) XY kymographs across the wound areas depicted in (**A-G**), respectively. Note wound overexpansion (yellow arrows); internal actin accumulation (yellow arrowhead), and remodeling defect/open wound (red arrowhead). (**H-N**) Quantification of wound area over time for (**A-G'**), respectively. Error bars represent $\pm$ SEM; n $\geq$ 10. Scale bars: 20 µm.

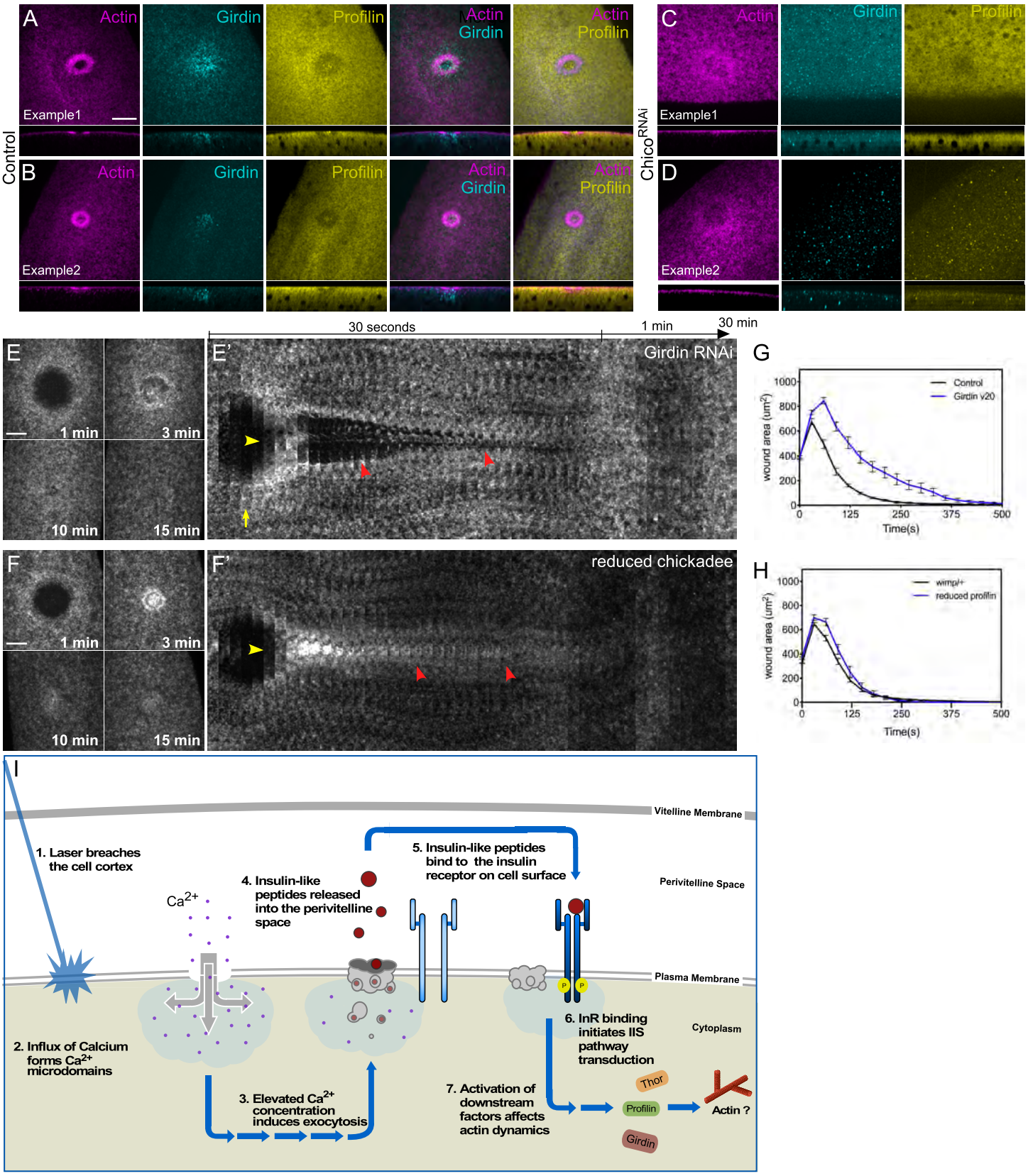
A
Actin
Girdin
Profilin
Actin Girdin
Actin Profilin
Example1
Control
B
Example2
C
Example1
ChicoRNAi
D
Example2
30 seconds
1 min
30 min
E
1 min
3 min
10 min
15 min
E'
Girdin RNAi
G
Control
Girdin v20
wound area (um²)
Time(s)
F
F'
reduced chickadee
H
wimpl+
reduced profilin
I
Vitelline Membrane
Perivitelline Space
Plasma Membrane
Cytoplasm
1. Laser breaches the cell cortex
2. Influx of Calcium forms Ca2+ microdomains
3. Elevated Ca2+ concentration induces exocytosis
4. Insulin-like peptides released into the perivitelline space
5. Insulin-like peptides bind to the insulin receptor on cell surface
6. InR binding initiates IIS pathway transduction
7. Activation of downstream factors affects actin dynamics
Thor
Profilin
Girdin
Actin ?

Figure 7. Chickadee (profilin) and Girdin are IIS pathway effectors during cell wound repair. (**A**-**D**) Confocal XY projections of laser wounded Drosophila NC4-6 wildtype (**A-B**) or *chico* RNAi knockdown (**C-D**) embryos stained for Girdin (Girdin), Chickadee/profilin (Profilin), and F-actin/phalloidin (Actin). (**E**-**F'**) Confocal XY projections of actin dynamics at 1, 5, 10, and 15 mpw from *Drosophila* NC4-6 embryos coexpressing sGMCA and a UAS-RNAi transgene during cell wound repair for Girdin^{RNAi} (Girdin^{RNAi}/+; sGMCA, 7063/+) (**E**) and reduced chickadee (sGMCA; *chickadee*^{221}/+ sGMCA, *wimp*/+) (**F**). (**E'**-**F'**) XY kymographs across the wound areas depicted in **E**-**F**, respectively. Note wound overexpansion (yellow arrows); internal actin accumulation (yellow arrowhead), and remodeling defect/open wound (red arrowhead). (**G-H**) Quantification of wound area over time for (**E**-**F'**), respectively. Error bars represent $\pm$ SEM; n $\geq$ 10. (**I**) Model for IIS pathway function in cell wound repair. Wounding of the cell cortex leads an rush of calcium into the cytoplasm developing locales of increased calcium concentration known as microdomains. To plug the hole, elevated calcium levels initiate exocytotic programs to recruit vescles to the wound area, forming a plug while simultaneously releasing insulin-like peptide 4 (ilp4) into the perivitelline space. Ilp4 is recognized by the insulin receptor (InR) where it binds and activates the IIS pathway. Subsequent phosphorylation events downstream of InR, ultimately activate downstream effectors including the actin remodelers Chickadee and Girdin to repair and restore the cortex back to its normal state. Scale bars: 20 μm.

Supplementary Figure S1. Knockdown of up-regulated genes results in wound overexpansion and abnormal actin dynamics. (**A-H**) Confocal XY projections of actin dynamics at 1, 5, 10, and 15 mpw from *Drosophila* NC4-6 embryos co-expressing sGMCA and a UAS-RNAi transgene during cell wound repair for Geko^{RNAi}/+; sGMCA,7063/+ (**A**), CG43693^{RNAi}/+; sGMCA,7063/+ (**B**), Dpn^{RNAi}/+; sGMCA,7063/+ (**C**), Link^{RNAi}/+; sGMCA,7063/+ (**D**), Ama^{RNAi}/+; sGMCA,7063/+ (**E**), l(3)neo38^{RNAi}/+; sGMCA,7063/+ (**F**), Danr^{RNAi}/+; sGMCA,7063/+ (**G**), and Dtg^{RNAi}/+; sGMCA,7063/+ (**H**). (**A'-H'**) XY kymographs across the wound areas depicted in (**A-H**), respectively. Note wound over-expansion (yellow arrows); internal actin accumulation (yellow arrowhead), and remodeling defect/open wound (red arrowhead). (**I-P**) Quantification of wound area over time for (**A-H'**), respectively. (**Q**) Quantification of RNAi efficiencies for each RNAi mutant background (2 biological and 2 technical replicates were performed). Error bars represent ± SEM; n ≥10. Side bars denote phenotypic classifiers: Class 1 (red), Class 2 (blue), Class 3 (green). Scale bars: 20 μm.

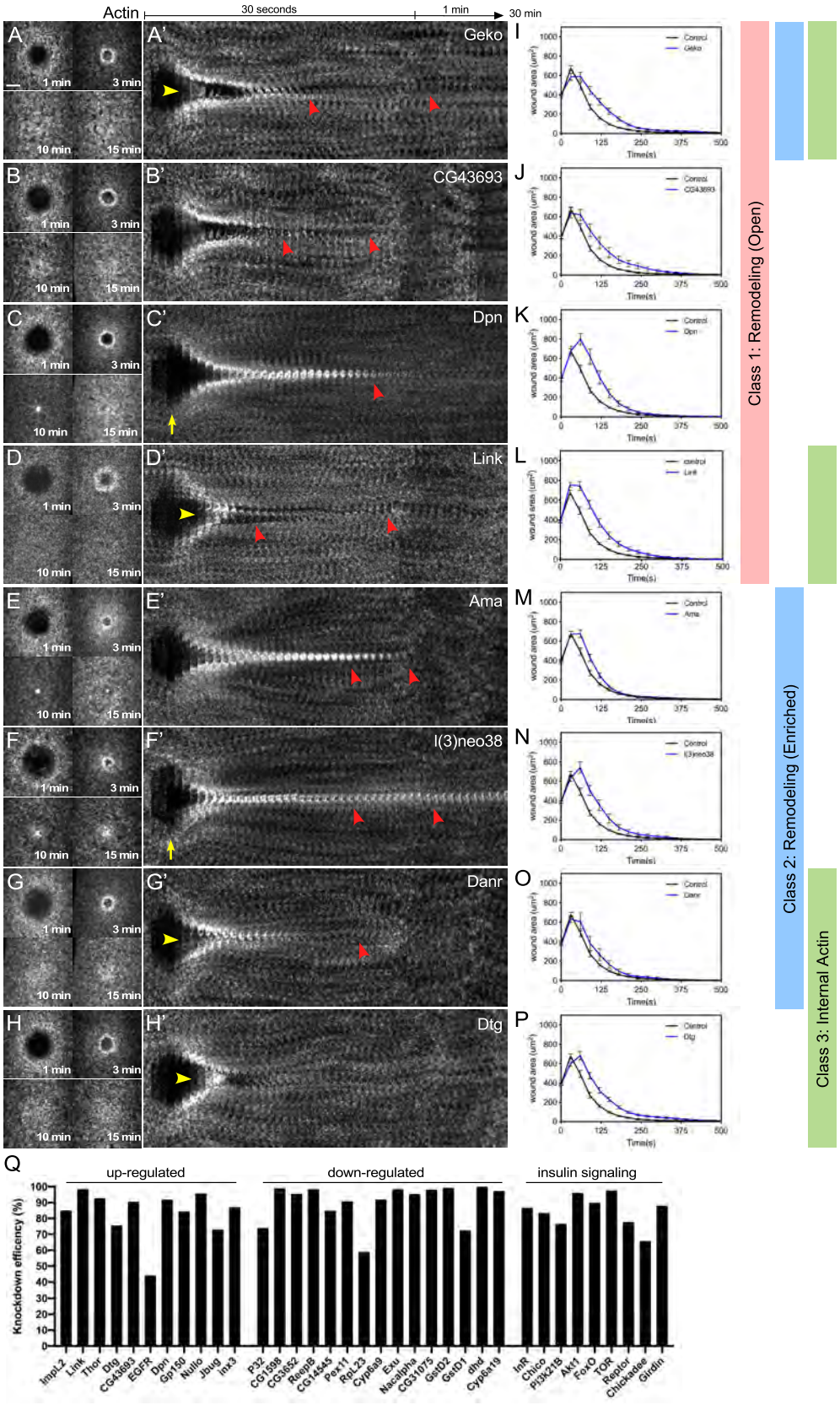
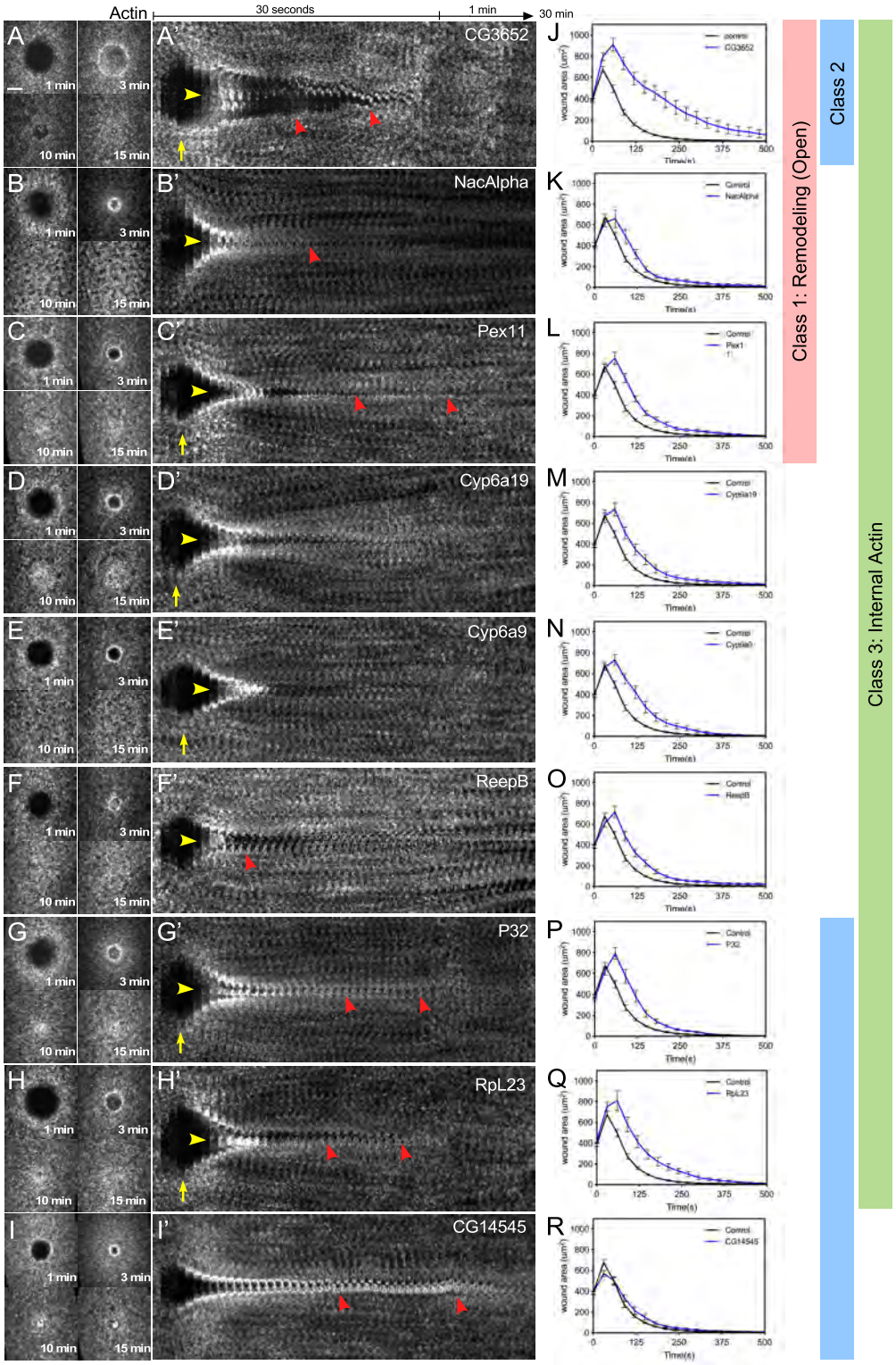
Supplementary Figure S2. Knockdown of down-regulated genes results in wound overexpansion and abnormal actin dynamics. (**A-I**) Confocal XY projections of actin dynamics at 1, 5, 10, and 15 mpw from *Drosophila* NC4-6 embryos co-expressing sGMCA and a UAS-RNAi transgene during cell wound repair for CG3652^{RNAi}/+; sGMCA,7063/+ (**A**), NacAlpha^{RNAi}/+; sGMCA,7063/+ (**B**), Pex11^{RNAi}/+; sGMCA,7063/+ (**C**), Cyp6a19^{RNAi}/+; sGMCA,7063/+ (**D**), Cyp6a9^{RNAi}/+; sGMCA,7063/+ (**E**), ReepB^{RNAi}/+; sGMCA,7063/+ (**F**), P32^{RNAi}/+; sGMCA,7063/+ (**G**), RpL23^{RNAi}/+; sGMCA,7063/+ (**H**), and CG14545^{RNAi}/+; sGMCA,7063/+ (**I**). (**A'-I'**) XY kymographs across the wound areas depicted in (A-**I**), respectively. Note wound over-expansion (yellow arrows); internal actin accumulation (yellow arrowhead), and remodeling defect/open wound (red arrowhead). (**J-R**) Quantification of wound area over time for (**A-I'**), respectively. Error bars represent ± SEM; n ≥10. Side bars denote phenotypic classifiers: Class 1 (red), Class 2 (blue), Class 3 (green). Scale bars: 20 μm.